Progress in modeling the impact of ICRF heating on high-Z impurity transport and turbulence stabilization

R. Bilato[1], C. Angioni[1], M. Brambilla[1], A. Di Siena[1], E. Fable[1], Vl. V. Bobkov[1], F. Casson[2], A. Kappatou[1], Ye. O. Kazakov[3], T. Görler[1], R. Ochoukov[1], E. Poli[1], M. Weiland[1], and the ASDEX Upgrade Team[4]

[1]Max-Planck-Institut für Plasmaphysik, Boltzmannstr. 2, Garching, Germany

[2]Culham Center for Fusion Energy, Culham Science Center, Abingdon, United Kingdom

[3]Laboratory for Plasma Physics, LPP-ERM/KMS, Brussels, Belgium

[4]H. Meyer et al. 2019 Nucl. Fusion 59 112014

18$^{\mathrm{th}}$ European Fusion Theory Conference, Ghent, 2019

Outline

1. Ion-Cyclotron Radio-Frequency (ICRF) heating
   - Modeling wave propagation & absorption
2. Impact of ICRF heating on the radial high-Z impurity transport
   - Neoclassical: T_i gradient and poloidal density asymmetries
   - Turbulence: affecting the electron to ion heat flux ratio
3. Effects of ICRF-accelerated fast ions on turbulence
   - ITG stabilization and T_i steepening in AUG discharge
   - Application to ITER
4. Validation (outlook)
5. Summary

Outline

1. Ion-Cyclotron Radio-Frequency (ICRF) heating
   - Modeling wave propagation & absorption
2. Impact of ICRF heating on the radial high-Z impurity transport
   - Neoclassical: T_i gradient and poloidal density asymmetries
   - Turbulence: affecting the electron to ion heat flux ratio
3. Effects of ICRF-accelerated fast ions on turbulence
   - ITG stabilization and T_i steepening in AUG discharge
   - Application to ITER
4. Validation (outlook)
5. Summary

1. ICRF Feature: Energetic Tails

Cyclotron Absorption

$$P_{\rm abs}^{(N)} \propto \left| E_+ \, J_{N-1}(k_\perp \rho) + e^{i\delta_k} E_- \, J_{N+1}(k_\perp \rho) \right|^2$$

($\rho = v_\perp \Omega_{\rm c}$ the Larmor radius; $\Omega_{\rm c} = Z_i e B / m_i c$)

- Ions – (*spatially localized*) cyclotron absorption at the Doppler-shifted resonance,

$$\omega \simeq N \, \Omega_c(\mathbf{r}) + k_\| v_\|$$

Cyclotron Absorption

$$P_{\mathrm{abs}}^{(N)} \propto \left| E_+ \, J_{N-1}(k_\perp \rho) + e^{i\delta_k} E_- \, J_{N+1}(k_\perp \rho) \right|^2$$

($\rho = v_\perp \Omega_c$ the Larmor radius; $\Omega_c = Z_i e B / m_i c$)

- Ions – (*spatially localized*) cyclotron absorption at the Doppler-shifted resonance,

$$\omega \simeq N \, \Omega_c(\mathbf{r}) + k_\parallel v_\parallel$$

- Electrons –(*spatially delocalized*) Landau-type resonances $\omega \simeq k_\parallel v_\parallel$; accelerated mainly by $\mathbf{E}_\parallel$.

Cyclotron Absorption

$$P_{\rm abs}^{(N)} \propto \left| E_+ \, J_{N-1}(k_\perp \rho) + e^{i\delta_k} E_- J_{N+1}(k_\perp \rho) \right|^2$$

($\rho = v_\perp \Omega_c$ the Larmor radius; $\Omega_c = Z_i e B / m_i c$)

- Ions – (*spatially localized*) cyclotron absorption at the Doppler-shifted resonance,

$$\omega \simeq N \, \Omega_c(\mathbf{r}) + k_\parallel v_\parallel$$

- Electrons –(*spatially delocalized*) Landau-type resonances $\omega \simeq k_\parallel v_\parallel$; accelerated mainly by $\mathbf{E}_\parallel$.

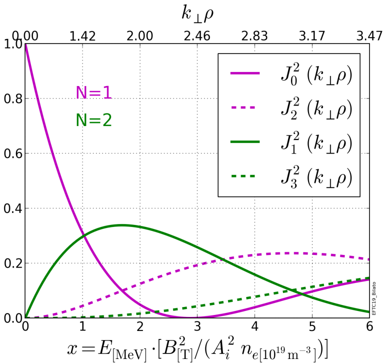

Cyclotron Absorption

$$P_{\text{abs}}^{(N)} \propto \left| E_+ \, J_{N-1}(k_\perp \rho) + e^{i\delta_k} E_- J_{N+1}(k_\perp \rho) \right|^2$$

($\rho = v_\perp \Omega_c$ the Larmor radius; $\Omega_c = Z_i e B / m_i c$)

- Ions – (*spatially localized*) cyclotron absorption at the Doppler-shifted resonance,

$$\omega \simeq N \, \Omega_c(\mathbf{r}) + k_\parallel v_\parallel$$

- Electrons –(*spatially delocalized*) Landau-type resonances $\omega \simeq k_\parallel v_\parallel$; accelerated mainly by $\mathbf{E}_\parallel$.

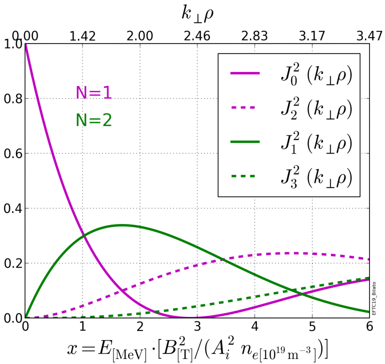

ICRF & energetic ions

ICRF heating can generate fast tails up to **MeV** energies (. . . stepwise).

2. ICRF Feature: Increase of the Trapping Fraction of the Resonant Species

- ICRF increases *on average* the perpendicular energy of the resonant ions:

2. ICRF Feature: Increase of the Trapping Fraction of the Resonant Species

- ICRF increases *on average* the perpendicular energy of the resonant ions:

GCENTER in TORIC-SSFPQL

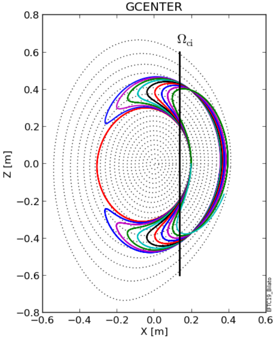

JET: γ-ray imaging(Kiptily, NF 2005)

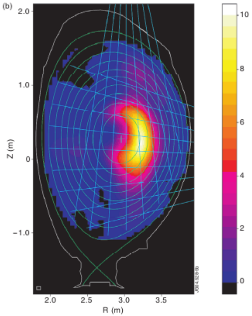

2. ICRF Feature: Increase of the Trapping Fraction of the Resonant Species

- ICRF increases *on average* the perpendicular energy of the resonant ions:

GCENTER in TORIC-SSFPQL

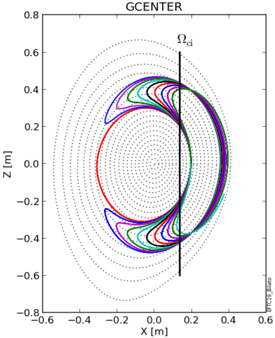

JET: γ-ray imaging(Kiptily, NF 2005)

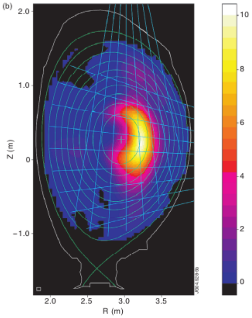

Consequences:

Accumulation of trapped ions with their *banana* tips on the Ω_{ic} resonance:

- Poloidally asymmetric density of the resonant ions $\Longrightarrow$ parallel pressure balance imposes a poloidal electric field pushing ions towards the HFS.

3. ICRF Feature: Collisional Electron Heating

- The critical (crossover) energy, $E_{\rm crt}$, above which the slowing down of energetic particles is mainly on electrons depend on the plasma composition

$$\frac{E_{\rm crt}}{T_e} \simeq 14.8\ A_m \left(\sum_i \frac{Z_i^2}{A_i} \frac{n_i}{n_e} \right)^{2/3}$$

$$A_m = M_m / m_p, \qquad q_m = Z_m\, e$$

3. ICRF Feature: Collisional Electron Heating

- The critical (crossover) energy, $E_{\rm crt}$, above which the slowing down of energetic particles is mainly on electrons depend on the plasma composition

$$\frac{E_{\rm crt}}{T_e} \simeq 14.8\, A_m \left(\sum_i \frac{Z_i^2}{A_i} \frac{n_i}{n_e} \right)^{2/3}$$

$$A_m = M_m/m_p, \qquad q_m = Z_m\, e$$

- This threshold is lower when the minority is H.

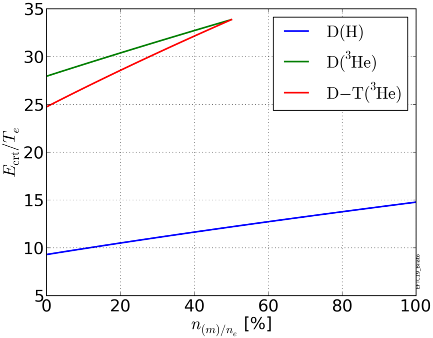

- The critical (crossover) energy, $E_{\rm crt}$, above which the slowing down of energetic particles is mainly on electrons depend on the plasma composition

$$\frac{E_{\rm crt}}{T_e} \simeq 14.8\ A_m \left(\sum_i \frac{Z_i^2}{A_i}\ \frac{n_i}{n_e} \right)^{2/3}$$

$$A_m = M_m/m_p, \qquad q_m = Z_m\ e$$

- This threshold is lower when the minority is H.

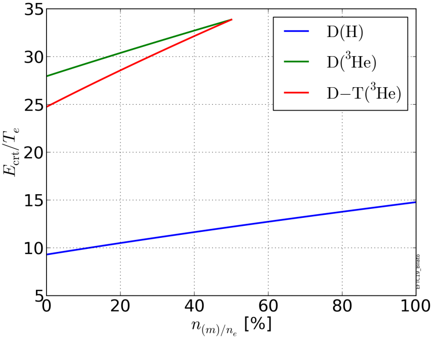

Consequence:

Even when most of the ICRF power is directly absorbed by ions,

- a **significant** fraction of the total absorbed ICRF power is collisionally transferred to electrons (higher in the case of H than of ^{3}He minority).

ICRF Modeling: Physics Workflow

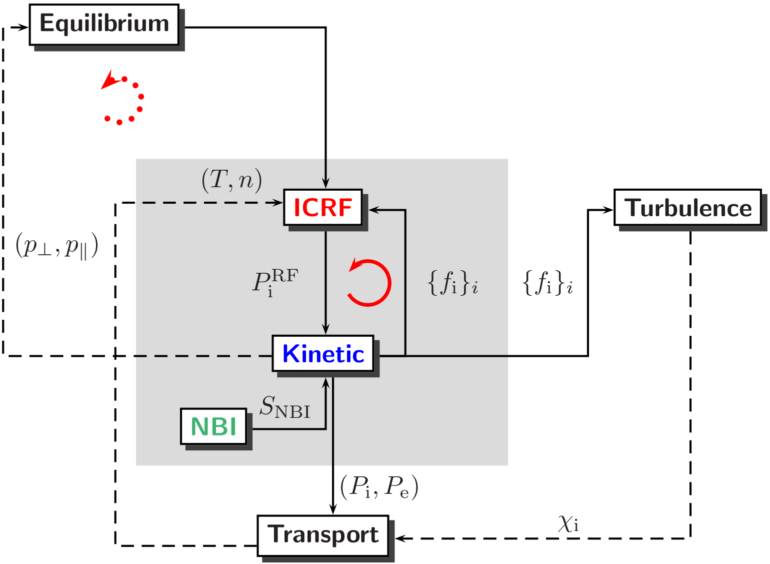

Outline

1. Ion-Cyclotron Radio-Frequency (ICRF) heating
   - Modeling wave propagation & absorption
2. Impact of ICRF heating on the radial high-Z impurity transport
   - Neoclassical: T_i gradient and poloidal density asymmetries
   - Turbulence: affecting the electron to ion heat flux ratio
3. Effects of ICRF-accelerated fast ions on turbulence
   - ITG stabilization and T_i steepening in AUG discharge
   - Application to ITER
4. Validation (outlook)
5. Summary

TORIC Solves the Wave Equation in Axisymmetric Plasmas

$$\vec{\nabla} \times \vec{\nabla} \times \vec{E} = \frac{\omega^2}{c^2}\left(\vec{E} + \frac{4\pi\, i}{\omega}(\tilde{\mathbf{j}}_{\mathrm{RF}} + \tilde{\mathbf{j}}_{\mathrm{ant}})\right) \quad \& \quad \text{b.c.}$$

(Brambilla, PPCF 1999)

TORIC in Brief

TORIC Solves the Wave Equation in Axisymmetric Plasmas

$$\vec{\nabla} \times \vec{\nabla} \times \vec{E} = \frac{\omega^2}{c^2} \left(\vec{E} + \frac{4\pi\, i}{\omega} (\tilde{\mathbf{j}}_{\mathrm{RF}} + \tilde{\mathbf{j}}_{\mathrm{ant}}) \right) \quad \& \quad \mathrm{b.c.}$$

(Brambilla, PPCF 1999)

- Minority, mode-conversion (Ion Bernstein (IBW) and Ion Cyclotron waves (ICW)), high-harmonics, and 3-ion heating schemes.

TORIC in Brief

TORIC Solves the Wave Equation in Axisymmetric Plasmas

$$\vec{\nabla} \times \vec{\nabla} \times \vec{E} = \frac{\omega^2}{c^2} \left(\vec{E} + \frac{4\pi\, i}{\omega} (\tilde{\mathbf{j}}_{\mathrm{RF}} + \tilde{\mathbf{j}}_{\mathrm{ant}}) \right) \quad \& \quad \text{b.c.}$$

(Brambilla, PPCF 1999)

- Minority, mode-conversion (Ion Bernstein (IBW) and Ion Cyclotron waves (ICW)), high-harmonics, and 3-ion heating schemes.
- Landau, TTMP, and mixed term for the electron damping.

TORIC in Brief

TORIC Solves the Wave Equation in Axisymmetric Plasmas

$$\vec{\nabla} \times \vec{\nabla} \times \vec{E} = \frac{\omega^2}{c^2}\left(\vec{E} + \frac{4\pi\, i}{\omega}(\tilde{\mathbf{j}}_{\mathrm{RF}} + \tilde{\mathbf{j}}_{\mathrm{ant}})\right) \quad \& \quad \mathrm{b.c.}$$

(Brambilla, PPCF 1999)

- Minority, mode-conversion (Ion Bernstein (IBW) and Ion Cyclotron waves (ICW)), high-harmonics, and 3-ion heating schemes.
- Landau, TTMP, and mixed term for the electron damping.
- Profiles of the driven current. (Ehst, NF 1991; Bilato, NF 2002)

TORIC in Brief

TORIC Solves the Wave Equation in Axisymmetric Plasmas

$$\vec{\nabla} \times \vec{\nabla} \times \vec{E} = \frac{\omega^2}{c^2} \left(\vec{E} + \frac{4\pi\, i}{\omega} (\tilde{\mathbf{j}}_{\rm RF} + \tilde{\mathbf{j}}_{\rm ant}) \right) \quad \& \quad \text{b.c.}$$

(Brambilla, PPCF 1999)

- Minority, mode-conversion (Ion Bernstein (IBW) and Ion Cyclotron waves (ICW)), high-harmonics, and 3-ion heating schemes.
- Landau, TTMP, and mixed term for the electron damping.
- Profiles of the driven current. (Ehst, NF 1991; Bilato, NF 2002)
- Profiles of the direct toroidal torque. (Bilato, NF 2017b)

TORIC in Brief

TORIC Solves the Wave Equation in Axisymmetric Plasmas

$$\vec{\nabla} \times \vec{\nabla} \times \vec{E} = \frac{\omega^2}{c^2}\left(\vec{E} + \frac{4\pi\, i}{\omega}(\tilde{\mathbf{j}}_{\rm RF} + \tilde{\mathbf{j}}_{\rm ant})\right) \quad \& \quad \text{b.c.}$$

(Brambilla, PPCF 1999)

- Minority, mode-conversion (Ion Bernstein (IBW) and Ion Cyclotron waves (ICW)), high-harmonics, and 3-ion heating schemes.
- Landau, TTMP, and mixed term for the electron damping.
- Profiles of the driven current. (Ehst, NF 1991; Bilato, NF 2002)
- Profiles of the direct toroidal torque. (Bilato, NF 2017b)
- Module for fusion alpha particles in DT plasmas (ITER and DEMO).
  (Bilato, JoP 2014; Brambilla, NF 2015)

TORIC Solves the Wave Equation in Axisymmetric Plasmas

$$\vec{\nabla} \times \vec{\nabla} \times \vec{E} = \frac{\omega^2}{c^2}\left(\vec{E} + \frac{4\pi\, i}{\omega}\left(\tilde{\mathbf{j}}_{\mathrm{RF}} + \tilde{\mathbf{j}}_{\mathrm{ant}}\right)\right) \quad \& \quad \text{b.c.}$$

(Brambilla, PPCF 1999)

- Minority, mode-conversion (Ion Bernstein (IBW) and Ion Cyclotron waves (ICW)), high-harmonics, and 3-ion heating schemes.
- Landau, TTMP, and mixed term for the electron damping.
- Profiles of the driven current. (Ehst, NF 1991; Bilato, NF 2002)
- Profiles of the direct toroidal torque. (Bilato, NF 2017b)
- Module for fusion alpha particles in DT plasmas (ITER and DEMO). (Bilato, JoP 2014; Brambilla, NF 2015)
- Antenna model for realistic spectrum of the antenna currents $\Longrightarrow$ estimate of the coupling resistance (scan in n_φ).

SSFPQL in Brief

SSFPQL: 2d Solver for the Steady-State Solution

$$\left(\frac{\partial F_i}{\partial t}\right)_{\mathrm{QL}} := \mathcal{Q}_{\mathrm{RF}}(F_i) + \mathcal{C}_{\mathrm{coll}}(F_i) + S_{\mathrm{NBI}} + L_{\mathrm{FIL}} \ldots = 0$$

(Brambilla, NF 1994)

SSFPQL in Brief

SSFPQL: 2d Solver for the Steady-State Solution

$$\left(\frac{\partial F_i}{\partial t}\right)_{\rm QL} := \mathcal{Q}_{\rm RF}(F_i) + \mathcal{C}_{\rm coll}(F_i) + S_{\rm NBI} + L_{\rm FIL} \ldots = 0$$

(Brambilla, NF 1994)

- Solved for **all** the **ions** with either $\mathcal{Q}_{\rm RF}(F_i) \neq 0$ or/and $S_{\rm NBI} \neq 0$.

SSFPQL in Brief

SSFPQL: 2d Solver for the Steady-State Solution

$$\left(\frac{\partial F_i}{\partial t}\right)_{\mathrm{QL}} := \mathcal{Q}_{\mathrm{RF}}(F_i) + \mathcal{C}_{\mathrm{coll}}(F_i) + S_{\mathrm{NBI}} + L_{\mathrm{FIL}} \ldots = 0$$

(Brambilla, NF 1994)

- Solved for **all** the **ions** with either $\mathcal{Q}_{\mathrm{RF}}(F_i) \neq 0$ or/and $S_{\mathrm{NBI}} \neq 0$.
- $\mathcal{Q}_{\mathrm{RF}}$ includes fundamental and harmonics absorption.

SSFPQL in Brief

SSFPQL: 2d Solver for the Steady-State Solution

$$\left(\frac{\partial F_i}{\partial t}\right)_{\mathrm{QL}} := \mathcal{Q}_{\mathrm{RF}}(F_i) + \mathcal{C}_{\mathrm{coll}}(F_i) + S_{\mathrm{NBI}} + L_{\mathrm{FIL}} \ldots = 0$$

(Brambilla, NF 1994)

- Solved for **all** the **ions** with either $\mathcal{Q}_{\mathrm{RF}}(F_i) \neq 0$ or/and $S_{\mathrm{NBI}} \neq 0$.
- $\mathcal{Q}_{\mathrm{RF}}$ includes fundamental and harmonics absorption.
- NBI source described with SINBAD code for ICRF-NBI synergies.

(Feng, CPC 1995; Bilato, NF 2011)

SSFPQL in Brief

SSFPQL: 2d Solver for the Steady-State Solution

$$\left(\frac{\partial F_i}{\partial t}\right)_{\rm QL} := \mathcal{Q}_{\rm RF}(F_i) + \mathcal{C}_{\rm coll}(F_i) + S_{\rm NBI} + L_{\rm FIL} \ldots = 0$$

(Brambilla, NF 1994)

- Solved for **all** the **ions** with either $\mathcal{Q}_{\rm RF}(F_i) \neq 0$ or/and $S_{\rm NBI} \neq 0$.
- $\mathcal{Q}_{\rm RF}$ includes fundamental and harmonics absorption.
- NBI source described with SINBAD code for ICRF-NBI synergies.

  (Feng, CPC 1995; Bilato, NF 2011)
- Upgraded by accounting for toroidal effects, e.g. **trapping** and **finite-orbit-width** (FOW) effects, particularly relevant for energetic particles (solver for guiding center trajectories).

  (Bilato, JoP 2012, AIP Conf. Proc. 2014; Belmondo, JoP 2010; A. Kappatou this conference)

SSFPQL in Brief

SSFPQL: 2d Solver for the Steady-State Solution

$$\left(\frac{\partial F_i}{\partial t}\right)_{\mathrm{QL}} := \mathcal{Q}_{\mathrm{RF}}(F_i) + \mathcal{C}_{\mathrm{coll}}(F_i) + S_{\mathrm{NBI}} + L_{\mathrm{FIL}} \ldots = 0$$

(Brambilla, NF 1994)

- Solved for **all** the **ions** with either $\mathcal{Q}_{\mathrm{RF}}(F_i) \neq 0$ or/and $S_{\mathrm{NBI}} \neq 0$.
- $\mathcal{Q}_{\mathrm{RF}}$ includes fundamental and harmonics absorption.
- NBI source described with SINBAD code for ICRF-NBI synergies.
  (Feng, CPC 1995; Bilato, NF 2011)
- Upgraded by accounting for toroidal effects, e.g. **trapping** and **finite-orbit-width** (FOW) effects, particularly relevant for energetic particles (solver for guiding center trajectories).
  (Bilato, JoP 2012, AIP Conf. Proc. 2014; Belmondo, JoP 2010; A. Kappatou this conference)
- Synthetic diagnostics for the neutron rate from fusion reactions, D+D but also with Be, crucial for ITER in the non-activated phase.
  (Bilato, NF 2011; Polevoi, IAEA 2019)

Coupling TORIC & SSFPQL

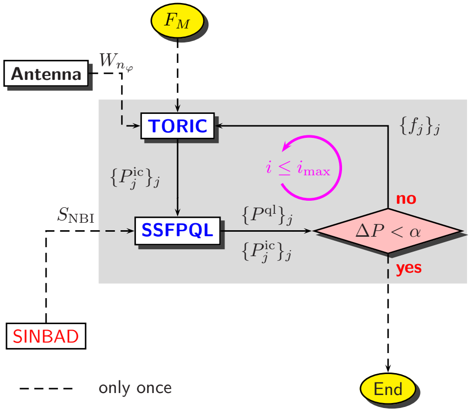

$$\Delta P = \max_i \left(\int |P^{\rm ic} - P^{\rm ql}| {\rm d}V \right)$$

(Brambilla, NF 2009, CPC 2013; Bilato, NF 2011)

Coupling TORIC & SSFPQL

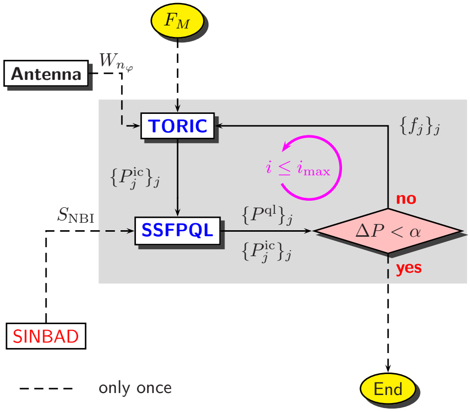

$$\Delta P = \max_i \left(\int |P^{\text{ic}} - P^{\text{ql}}| \mathrm{d}V \right)$$

(Brambilla, NF 2009, CPC 2013; Bilato, NF 2011)

- Initial Step: Maxwellians with the input temperatures.

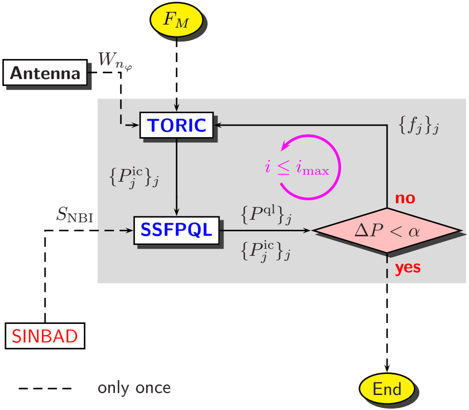

$$\Delta P = \max_i \left(\int |P^{\rm ic} - P^{\rm ql}| {\rm d}V \right)$$

(Brambilla, NF 2009, CPC 2013; Bilato, NF 2011)

- Initial Step: Maxwellians with the input temperatures.
- SSFPQL uses $P_j^{\rm ic}(\rho)$ for the quasilinear operator.

Coupling TORIC & SSFPQL

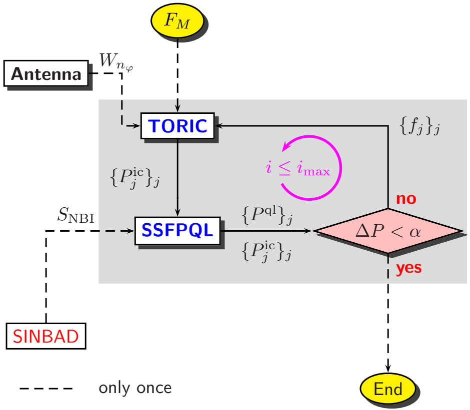

$$\Delta P = \max_i \left(\int |P^{\rm ic} - P^{\rm ql}| {\rm d}V \right)$$

(Brambilla, NF 2009, CPC 2013; Bilato, NF 2011)

- Initial Step: Maxwellians with the input temperatures.
- SSFPQL uses $P_j^{\rm ic}(\rho)$ for the quasilinear operator.
- The numerical $\{f_j\}_j$ is used in TORIC for the coefficients of the wave equation.

Coupling TORIC & SSFPQL

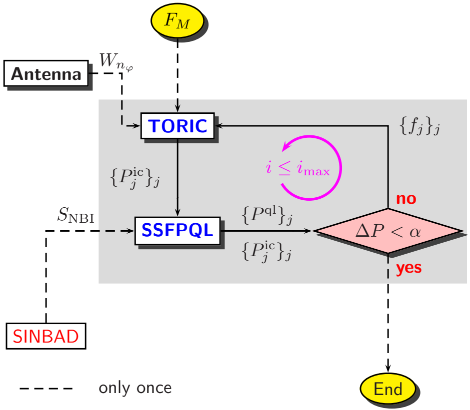

$$\Delta P = \max_i \left(\int |P^{\rm ic} - P^{\rm ql}| {\rm d}V \right)$$

(Brambilla, NF 2009, CPC 2013; Bilato, NF 2011)

- Initial Step: Maxwellians with the input temperatures.
- SSFPQL uses $P_j^{\rm ic}(\rho)$ for the quasilinear operator.
- The numerical $\{f_j\}_j$ is used in TORIC for the coefficients of the wave equation.
- The loop controller is the difference between the absorbed powers calculated by the two codes: α is decided by the user.

Coupling TORIC & SSFPQL

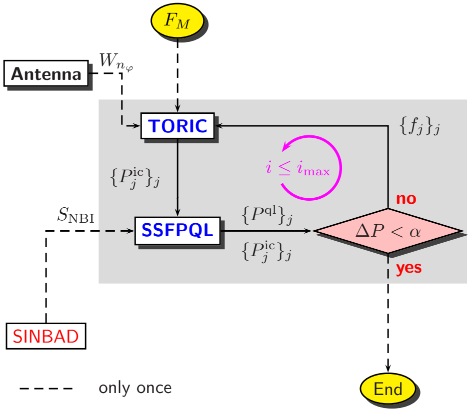

$$\Delta P = \max_i \left(\int |P^{\rm ic} - P^{\rm ql}| {\rm d}V \right)$$

(Brambilla, NF 2009, CPC 2013; Bilato, NF 2011)

- Initial Step: Maxwellians with the input temperatures.
- SSFPQL uses $P_j^{\rm ic}(\rho)$ for the quasilinear operator.
- The numerical $\{f_j\}_j$ is used in TORIC for the coefficients of the wave equation.
- The loop controller is the difference between the absorbed powers calculated by the two codes: α is decided by the user.
- Antenna module gives the weight of each toroidal component n_φ.

TORIC-SSFPQL Loop: an Example

(5% of H in D plasma and $P_{\mathrm{icrf}} = 4$ MW)

Without NBI

With D-NBI

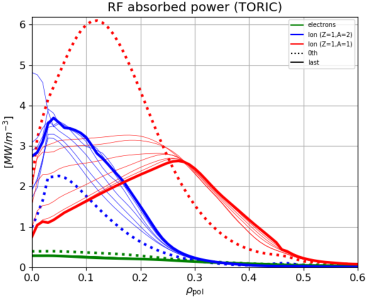

TORIC-SSFPQL Loop: an Example

(5% of H in D plasma and $P_{\mathrm{icrf}} = 4$ MW)

Without NBI

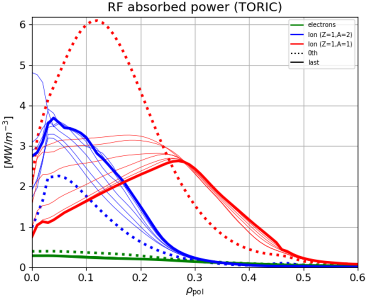

With D-NBI

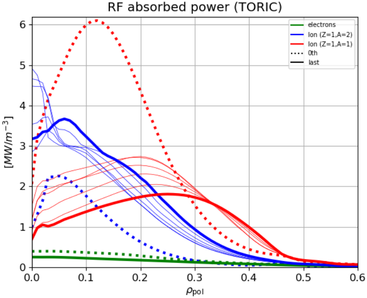

TORIC-SSFPQL Loop: an Example

(5% of H in D plasma and $P_{\mathrm{icrf}} = 4$ MW)

Without NBI

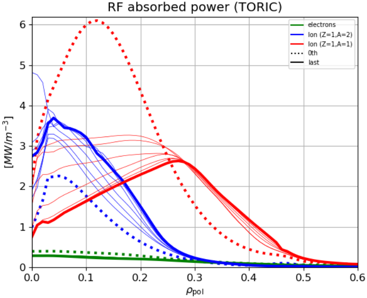

With D-NBI

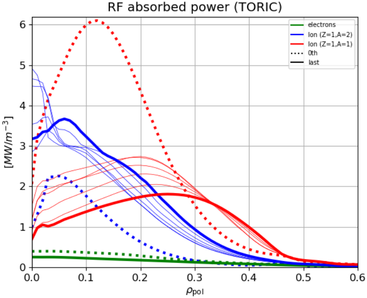

- ICRF-induced deviations of the dist. fun. from the Maxwellian modify both the radial profile and the amplitude of the ICRF absorbed power.
- NBI species resonating with the waves can substantially modify the distribution function and thus the ICRF absorption pattern.

Outline

1. Ion-Cyclotron Radio-Frequency (ICRF) heating
   - Modeling wave propagation & absorption
2. Impact of ICRF heating on the radial high-Z impurity transport
   - Neoclassical: T_i gradient and poloidal density asymmetries
   - Turbulence: affecting the electron to ion heat flux ratio
3. Effects of ICRF-accelerated fast ions on turbulence
   - ITG stabilization and T_i steepening in AUG discharge
   - Application to ITER
4. Validation (outlook)
5. Summary

High-Z Impurity Accumulation

- High-Z impurity accumulation in the plasma core can
  - increase the radiative losses $\Longrightarrow$ thermal-quench;
  - dilute the fusion fuel $\Longrightarrow$ downgrade the reactor performances.

High-Z Impurity Accumulation

- High-Z impurity accumulation in the plasma core can
  - increase the radiative losses $\Longrightarrow$ thermal-quench;
  - dilute the fusion fuel $\Longrightarrow$ downgrade the reactor performances.
- High-Z impurity accumulation results from the complex interplay between **neoclassical** (NC) and **turbulent** transport.

High-Z Impurity Accumulation

- High-Z impurity accumulation in the plasma core can
  - increase the radiative losses $\Longrightarrow$ thermal-quench;
  - dilute the fusion fuel $\Longrightarrow$ downgrade the reactor performances.
- High-Z impurity accumulation results from the complex interplay between **neoclassical** (NC) and **turbulent** transport.

ICRF heating can influence the high-Z impurity accumulation

- by acting on the neoclassical contribution;

High-Z Impurity Accumulation

- High-Z impurity accumulation in the plasma core can
  - increase the radiative losses $\Longrightarrow$ thermal-quench;
  - dilute the fusion fuel $\Longrightarrow$ downgrade the reactor performances.
- High-Z impurity accumulation results from the complex interplay between **neoclassical** (NC) and **turbulent** transport.

ICRF heating can influence the high-Z impurity accumulation

- by acting on the neoclassical contribution;
- by influencing *turbulence* which counteracts the inward NC convection.

In the limit of large aspect ratio, $\epsilon \ll 1$, $B \simeq B_0(1 - \epsilon \cos\vartheta) + \mathcal{O}(\epsilon^2)$;

Radial Pfirsch-Schlüter flux (high collisionality)

- **Toroidicity:** the *diamagnetic* component of the particle flux is not divergence free $\Longrightarrow$ a parallel return flux for the continuity equation.

In the limit of large aspect ratio, $\epsilon \ll 1$, $B \simeq B_0(1-\epsilon\cos\vartheta)+\mathcal{O}(\epsilon^2)$;

Radial Pfirsch-Schlüter flux (high collisionality)

- **Toroidicity:** the *diamagnetic* component of the particle flux is not divergence free $\Longrightarrow$ a parallel return flux for the continuity equation.
- **Collisionality** ($\propto Z^2$): The collisional friction on this *parallel flux* causes the radial Pfirsch-Schlüter (PS) flux: it varies on the magnetic surface, inward on the *inboard* side, and outward on the *outboard* side.

Neoclassical Pfirsch-Schlüter Flux

In the limit of large aspect ratio, $\epsilon \ll 1$, $B \simeq B_0(1 - \epsilon \cos\vartheta) + \mathcal{O}(\epsilon^2)$;

Radial Pfirsch-Schlüter flux (high collisionality)

- **Toroidicity:** the *diamagnetic* component of the particle flux is not divergence free $\Longrightarrow$ a parallel return flux for the continuity equation.
- **Collisionality** ($\propto Z^2$)**:** The collisional friction on this *parallel flux* causes the radial Pfirsch-Schlüter (PS) flux: it varies on the magnetic surface, inward on the *inboard* side, and outward on the *outboard* side.
  - Locally on a magnetic surface the PS flux is relatively large, $\mathcal{O}(q_{\rm sf}^2/\epsilon)$, with $q_{\rm sf}$ the safety factor.

Neoclassical Pfirsch-Schlüter Flux

In the limit of large aspect ratio, $\epsilon \ll 1$, $B \simeq B_0(1 - \epsilon \cos\vartheta) + \mathcal{O}(\epsilon^2)$;

Radial Pfirsch-Schlüter flux (high collisionality)

- **Toroidicity:** the *diamagnetic* component of the particle flux is not divergence free $\Longrightarrow$ a parallel return flux for the continuity equation.
- **Collisionality** ($\propto Z^2$): The collisional friction on this *parallel flux* causes the radial Pfirsch-Schlüter (PS) flux: it varies on the magnetic surface, inward on the *inboard* side, and outward on the *outboard* side.
  - Locally on a magnetic surface the PS flux is relatively large, $\mathcal{O}(q_{\rm sf}^2/\epsilon)$, with $q_{\rm sf}$ the safety factor.
  - However, the surface-averaged PS flux is ε–smaller than the local value, $\mathcal{O}(q_{\rm sf}^2)$ (because of large compensations!!!).

Neoclassical Pfirsch-Schlüter Flux

In the limit of large aspect ratio, $\epsilon \ll 1$, $B \simeq B_0(1 - \epsilon \cos\vartheta) + \mathcal{O}(\epsilon^2)$;

Radial Pfirsch-Schlüter flux (high collisionality)

- **Toroidicity:** the *diamagnetic* component of the particle flux is not divergence free $\Longrightarrow$ a parallel return flux for the continuity equation.
- **Collisionality** ($\propto Z^2$): The collisional friction on this *parallel flux* causes the radial Pfirsch-Schlüter (PS) flux: it varies on the magnetic surface, inward on the *inboard* side, and outward on the *outboard* side.
  - Locally on a magnetic surface the PS flux is relatively large, $\mathcal{O}(q_{\rm sf}^2/\epsilon)$, with $q_{\rm sf}$ the safety factor.
  - However, the surface-averaged PS flux is ε–smaller than the local value, $\mathcal{O}(q_{\rm sf}^2)$ (because of large compensations!!!).
- **Ambipolarity** (momentum conservation&quasineutrality): $\Gamma_Z \approx -\Gamma_i/Z$, the main-ion PS flux is balanced by the high-Z radial flux.

(Helander&Sigmar 2002)

Neoclassical PS Flux of High-Z Impurities

High-Z PS flux

$$\frac{R\,\langle \boldsymbol{\Gamma}_Z^{\rm neo}\cdot\nabla r\rangle}{\langle n_Z\rangle} \approx D_{\rm PS,i}\, Z\left[\left(\frac{{\rm d}\ln p_i}{{\rm d}r} - \frac{T_Z}{Z\,T_i}\frac{{\rm d}\ln p_Z}{{\rm d}r}\right) - \frac{3}{2}\frac{{\rm d}\ln T_i}{{\rm d}r}\right]$$

$$\approx D_{\rm PS,i}\, Z\left[-\frac{R}{L_{n_i}} + \frac{1}{2}\frac{R}{L_{T_i}}\right] = D_{\rm PS,i}\frac{R}{L_{n_i}}\, Z\left(-1+\frac{\eta_i}{2}\right)$$

with: $D_{\rm PS} = q_{\rm sf}^2\,\nu_{c,i}\langle\rho_i^{-1}\rangle^{-1}$ **PS diffusion coefficient** of main ions;
$L_A = -A^{-1}{\rm d}A/{\rm d}r$, and $L_A > 0$ when A peaked in the core;
$\langle\boldsymbol{\Gamma}_Z^{\rm neo}\cdot\nabla r\rangle > 0$ when the flux points outwards;
$\langle\cdots\rangle$ surface average;
terms $\propto R/L_{T_i}$ are known as temperature screening contribution.

High-Z PS flux

$$\frac{R\,\langle \mathbf{\Gamma}_Z^{\rm neo}\cdot\nabla r\rangle}{\langle n_Z\rangle} \approx D_{\rm PS,i}\; Z\left[\left(\frac{{\rm d}\ln p_i}{{\rm d}r} - \frac{T_Z}{Z\,T_i}\frac{{\rm d}\ln p_Z}{{\rm d}r}\right) - \frac{3}{2}\frac{{\rm d}\ln T_i}{{\rm d}r}\right]$$

$$\approx D_{\rm PS,i}\; Z\left[-\frac{R}{L_{n_i}} + \frac{1}{2}\frac{R}{L_{T_i}}\right] = D_{\rm PS,i}\frac{R}{L_{n_i}}\; Z\left(-1+\frac{\eta_i}{2}\right)$$

with: $D_{\rm PS} = q_{\rm sf}^2\,\nu_{c,i}\langle\rho_i^{-1}\rangle^{-1}$ **PS diffusion coefficient** of main ions;
$L_A = -A^{-1}{\rm d}A/{\rm d}r$, and $L_A > 0$ when A peaked in the core;
$\langle\mathbf{\Gamma}_Z^{\rm neo}\cdot\nabla r\rangle > 0$ when the flux points outwards;
$\langle\cdots\rangle$ surface average;
terms $\propto R/L_{T_i}$ are known as temperature screening contribution.

Null-condition for the PS flux $\langle\mathbf{\Gamma}_Z^{\rm neo}\cdot\nabla r\rangle = 0$

The PS flux is zero when $\eta_i = L_{n_i}/L_{T_i} = 2$:
$\Longrightarrow$ temperature more peaked than density.

PS Flux in a Poloidally Inhomogeneous Density

Collisionality depends on the **local** density: which is the influence of poloidally inhomogeneous n_Z on the PS flux (due to the *large compensations*)?

PS Flux in a Poloidally Inhomogeneous Density

Collisionality depends on the **local** density: which is the influence of poloidally inhomogeneous n_Z on the PS flux (due to the *large compensations*)?

Poloidal asymmetry model: $n_z = 1 + \delta \cos(\vartheta)$ & main ions in banana regime.

PS Flux in a Poloidally Inhomogeneous Density

Collisionality depends on the **local** density: which is the influence of poloidally inhomogeneous n_Z on the PS flux (due to the *large compensations*)?

Poloidal asymmetry model: $n_z = 1 + \delta \cos(\vartheta)$ & main ions in banana regime.

High-Z PS flux in a poloidally inhomogeneous density

$$\frac{R \langle \mathbf{\Gamma}_Z^{\rm neo} \cdot \nabla r \rangle}{\langle n_Z \rangle D_{\rm PS,i} (R/L_{n_i})} \approx Z \left\{ \left[1 + \frac{\delta}{\epsilon} + \frac{1}{4}\frac{\delta^2}{\epsilon^2} \right] \left(-1 + \frac{\eta_i}{2} \right) - \left[\frac{\delta}{\epsilon} + \frac{1}{2}\frac{\delta^2}{\epsilon^2} \right] \frac{f_c}{3} \frac{\eta_i}{2} \right\}$$

with $f_c \approx 1 - 1.46\sqrt{\epsilon}$ the fraction of circulating ions ($0.18 \lesssim f_c \lesssim 1$).

PS Flux in a Poloidally Inhomogeneous Density

Collisionality depends on the **local** density: which is the influence of poloidally inhomogeneous n_Z on the PS flux (due to the *large compensations*)?

Poloidal asymmetry model: $n_z = 1 + \delta\cos(\vartheta)$ & main ions in banana regime.

High-Z PS flux in a poloidally inhomogeneous density

$$\frac{R\left\langle \mathbf{\Gamma}_Z^{\rm neo}\cdot\nabla r\right\rangle}{\langle n_Z\rangle D_{\rm PS,i}(R/L_{n_i})} \approx Z\left\{\left[1+\frac{\delta}{\epsilon}+\frac{1}{4}\frac{\delta^2}{\epsilon^2}\right]\left(-1+\frac{\eta_i}{2}\right)-\left[\frac{\delta}{\epsilon}+\frac{1}{2}\frac{\delta^2}{\epsilon^2}\right]\frac{f_c}{3}\frac{\eta_i}{2}\right\}$$

with $f_c \approx 1-1.46\sqrt{\epsilon}$ the fraction of circulating ions $(0.18 \lesssim f_c \lesssim 1)$.

Rotating plasmas $\delta/\epsilon \gg 1$

Centrifugal forces are particularly strong for high-Z impurities (high masses) $\Longrightarrow \delta/\epsilon \gg 1$ ($\delta/\epsilon \approx A_z M_{\varphi,p}^2 \lesssim 6$ for W in ASDEX-Upgrade (AUG), $M_{\varphi,p}$ proton Mach number).

(Angioni, PPCF 2014)

Null-Point of PS Flux

High-Z PS flux in a poloidally inhomogeneous density

$$\frac{R\,\langle \boldsymbol{\Gamma}_Z^{\rm neo}\cdot\nabla r\rangle}{\langle n_Z\rangle\, D_{\rm PS,i}(R/L_{n_i})} \approx Z\left\{\left[1+\frac{\delta}{\epsilon}+\frac{1}{4}\frac{\delta^2}{\epsilon^2}\right]\left(-1+\frac{\eta_i}{2}\right)-\left[\frac{\delta}{\epsilon}+\frac{1}{2}\frac{\delta^2}{\epsilon^2}\right]\;\frac{f_c}{3}\;\frac{\eta_i}{2}\right\}$$

Null-Point of PS Flux

High-Z PS flux in a poloidally inhomogeneous density

$$\frac{R\,\langle \mathbf{\Gamma}_Z^{\rm neo}\cdot\nabla r\rangle}{\langle n_Z\rangle\, D_{\rm PS,i}(R/L_{n_i})} \approx Z\left\{\left[1+\frac{\delta}{\epsilon}+\frac{1}{4}\frac{\delta^2}{\epsilon^2}\right]\left(-1+\frac{\eta_i}{2}\right)-\left[\frac{\delta}{\epsilon}+\frac{1}{2}\frac{\delta^2}{\epsilon^2}\right]\frac{f_c}{3}\,\frac{\eta_i}{2}\right\}$$

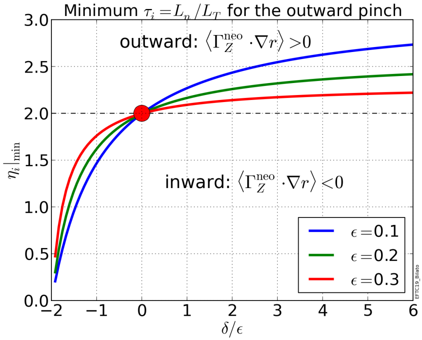

Null-Point of PS Flux

High-Z PS flux in a poloidally inhomogeneous density

$$\frac{R\,\langle \mathbf{\Gamma}_Z^{\rm neo}\cdot\nabla r\rangle}{\langle n_Z\rangle\, D_{\rm PS,i}(R/L_{n_i})} \approx Z\left\{\left[1+\frac{\delta}{\epsilon}+\frac{1}{4}\frac{\delta^2}{\epsilon^2}\right]\left(-1+\frac{\eta_i}{2}\right)-\left[\frac{\delta}{\epsilon}+\frac{1}{2}\frac{\delta^2}{\epsilon^2}\right]\frac{f_c}{3}\frac{\eta_i}{2}\right\}$$

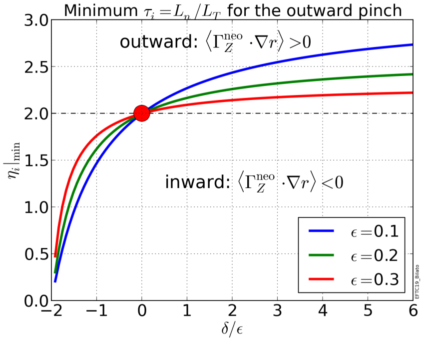

- Out-In $(\delta > 0) \Longrightarrow$ increases $\eta_i|_{\rm min}$: Collisionality of main ions with high-Z impurity larger on the outboard $\Longrightarrow$ outwards main-ion diffusion compensated by an inward high-Z diffusion.

Null-Point of PS Flux

High-Z PS flux in a poloidally inhomogeneous density

$$\frac{R\,\langle \mathbf{\Gamma}_Z^{\rm neo}\cdot\nabla r\rangle}{\langle n_Z\rangle\, D_{\rm PS,i}(R/L_{n_i})} \approx Z\left\{\left[1+\frac{\delta}{\epsilon}+\frac{1}{4}\frac{\delta^2}{\epsilon^2}\right]\left(-1+\frac{\eta_i}{2}\right)-\left[\frac{\delta}{\epsilon}+\frac{1}{2}\frac{\delta^2}{\epsilon^2}\right]\frac{f_c}{3}\frac{\eta_i}{2}\right\}$$

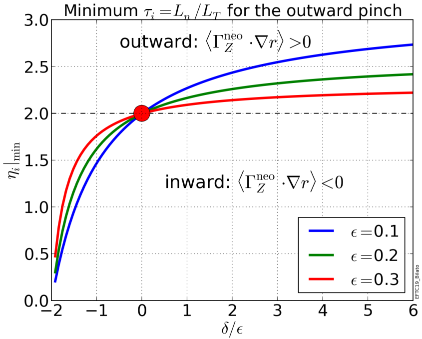

- Out-In $(\delta > 0) \Longrightarrow$ increases $\eta_i|_{\rm min}$: Collisionality of main ions with high-Z impurity larger on the outboard $\Longrightarrow$ outwards main-ion diffusion compensated by an inward high-Z diffusion.
- In-Out $(\delta < 0) \Longrightarrow$ reduces $\eta_i|_{\rm min}$. (viceversa of Out-In)

Null-Point of PS Flux

High-Z PS flux in a poloidally inhomogeneous density

$$\frac{R\,\langle \mathbf{\Gamma}_Z^{\rm neo}\cdot\nabla r\rangle}{\langle n_Z\rangle\, D_{\rm PS,i}(R/L_{n_i})} \approx Z\left\{\left[1+\frac{\delta}{\epsilon}+\frac{1}{4}\frac{\delta^2}{\epsilon^2}\right]\left(-1+\frac{\eta_i}{2}\right)-\left[\frac{\delta}{\epsilon}+\frac{1}{2}\frac{\delta^2}{\epsilon^2}\right]\frac{f_c}{3}\frac{\eta_i}{2}\right\}$$

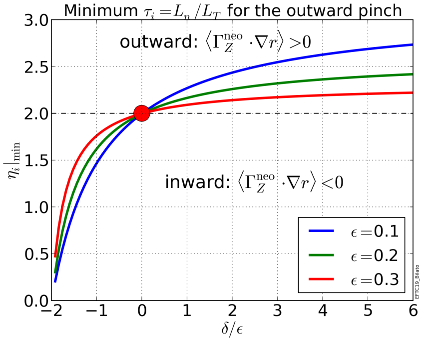

- Out-In $(\delta > 0) \Longrightarrow$ increases $\eta_i|_{\rm min}$: Collisionality of main ions with high-Z impurity larger on the outboard $\Longrightarrow$ outwards main-ion diffusion compensated by an inward high-Z diffusion.
- In-Out $(\delta < 0) \Longrightarrow$ reduces $\eta_i|_{\rm min}$. (viceversa of Out-In)

In-Out $(\delta \lesssim 0)$ asymmetry of n_z is preferable to avoid Z accumulation in the plasma core.

Outline

1. Ion-Cyclotron Radio-Frequency (ICRF) heating
   - Modeling wave propagation & absorption
2. Impact of ICRF heating on the radial high-Z impurity transport
   - Neoclassical: T_i gradient and poloidal density asymmetries
   - Turbulence: affecting the electron to ion heat flux ratio
3. Effects of ICRF-accelerated fast ions on turbulence
   - ITG stabilization and T_i steepening in AUG discharge
   - Application to ITER
4. Validation (outlook)
5. Summary

How ICRF Heating Can Impact the NC Transport

- $\boxed{\eta}$: The ICRF–heated ions contribute to the *temperature screening*,

$$\eta \approx \eta_i + \nu_{ic}\, \eta_{\rm ic}$$

where $\nu_{ic} = n_{\rm ic}/n_e \ll 1$ is the concentration of the ICRF heated ions.

- $\boxed{\delta/\epsilon}$: ICRF heating increases the fraction of trapped ion of the resonating species $\Rightarrow$ outboard accumulation of resonating ions $\Rightarrow$ parallel pressure balance imposes a poloidal electric field pushing ions towards the HFS $\Rightarrow$ effective on high-Z impurities.

(Reinke, PPCF 2012; Casson, PPCF 2015)

How ICRF Heating Can Impact the NC Transport

- $\boxed{\eta}$: The ICRF–heated ions contribute to the *temperature screening*,

$$\eta \approx \eta_i + \nu_{ic}\, \eta_{\rm ic}$$

where $\nu_{ic} = n_{\rm ic}/n_e \ll 1$ is the concentration of the ICRF heated ions.

- $\boxed{\delta/\epsilon}$: ICRF heating increases the fraction of trapped ion of the resonating species $\Rightarrow$ outboard accumulation of resonating ions $\Rightarrow$ parallel pressure balance imposes a poloidal electric field pushing ions towards the HFS $\Rightarrow$ effective on high-Z impurities.

(Reinke, PPCF 2012; Casson, PPCF 2015)

ICRF-Induced In-Out Asymmetry

Impurity Density Variation due to ICRF and Plasma Rotation

$$\ln\left(\frac{n_Z}{n_{Z,\mathrm{LFS}}}\right) \approx -Z_Z \frac{Z_{\mathrm{ic}} T_e}{T_i + Z_{\mathrm{eff}} T_e} \frac{n_{\mathrm{ic}} - n_{\mathrm{ic,LFS}}}{n_e} + \ \ldots (\mathrm{ICRF})$$

$$\frac{m_Z V_\varphi^2}{2T_i}\left[1 - Z_Z \frac{m_{\mathrm{eff}}}{m_Z} \frac{T_e}{T_i + Z_{\mathrm{eff}} T_e}\right]\left(1 - \frac{R_{\mathrm{LFS}}^2}{R^2}\right) \ \ldots (\mathrm{Centrifugal})$$

ICRF-Induced In-Out Asymmetry

Impurity Density Variation due to ICRF and Plasma Rotation

$$\ln\left(\frac{n_Z}{n_{Z,\mathrm{LFS}}}\right) \approx -Z_Z \frac{Z_{\mathrm{ic}} T_e}{T_i + Z_{\mathrm{eff}} T_e} \frac{n_{\mathrm{ic}} - n_{\mathrm{ic,LFS}}}{n_e} + \ \ldots (\mathrm{ICRF})$$

$$\frac{m_Z V_\varphi^2}{2T_i}\left[1 - Z_Z \frac{m_{\mathrm{eff}}}{m_Z} \frac{T_e}{T_i + Z_{\mathrm{eff}} T_e}\right]\left(1 - \frac{R_{\mathrm{LFS}}^2}{R^2}\right) \ \ldots (\mathrm{Centrifugal})$$

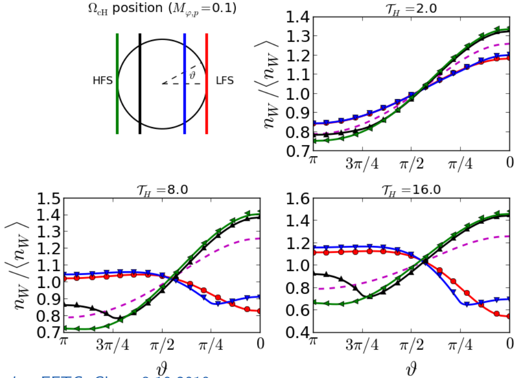

$\mathcal{T}_H = \frac{T_\perp}{T_\parallel}$ at the Ω_{cH} resonance.

(Bilato, NF 2014, NF 2017a)

Dependence on the Plasma Rotation

The ICRF in-out asymmetry has a noticeable effect if the toroidal plasma velocity, V_φ, is not too large,

$$V_\varphi < 310 \sqrt{\frac{n_{\mathrm{ic}}}{n_e} \, \frac{Z_Z}{A_Z}\left(1 - \frac{Z_Z}{A_Z}\right)^{-1} T_{i\,[\mathrm{keV}]}} \, \frac{\mathrm{km}}{\mathrm{s}} \approx 100 \frac{\mathrm{km}}{\mathrm{s}}$$

$$M_\varphi < \sqrt{\frac{n_{\mathrm{ic}}}{n_e} \, \frac{Z_Z}{A_Z}\left(1 - \frac{Z_Z}{A_Z}\right)^{-1}}$$

Dependence on the Plasma Rotation

The ICRF in-out asymmetry has a noticeable effect if the toroidal plasma velocity, V_φ, is not too large,

$$V_\varphi < 310\sqrt{\frac{n_{\rm ic}}{n_e}\,\frac{Z_Z}{A_Z}\left(1-\frac{Z_Z}{A_Z}\right)^{-1} T_{i\,[\rm keV]}}\;\frac{\rm km}{\rm s} \approx 100\frac{\rm km}{\rm s}$$

$$M_\varphi < \sqrt{\frac{n_{\rm ic}}{n_e}\,\frac{Z_Z}{A_Z}\left(1-\frac{Z_Z}{A_Z}\right)^{-1}}$$

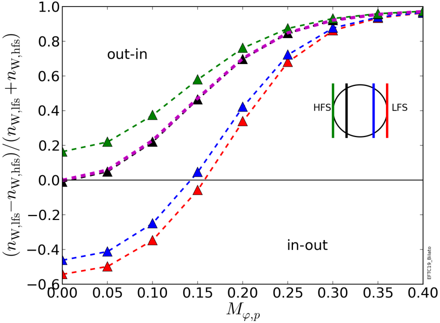

- barely satisfied in NBI-heated medium-size plasmas;
- more easily satisfied in fusion reactor plasmas.

(Bilato, NF 2014, NF 2017a)

Example: ASDEX-Upgrade #30812@4.6

Only NBI

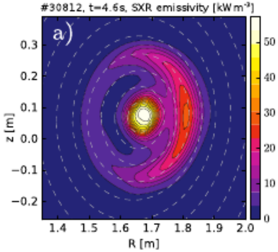

NBI+ICRF

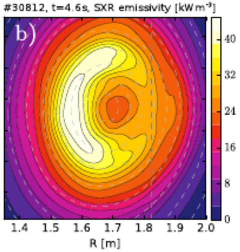

Example: ASDEX-Upgrade #30812@4.6

Only NBI

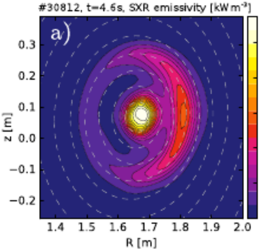

NBI+ICRF

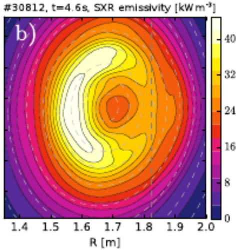

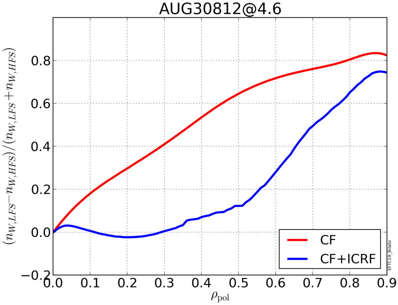

TORIC-SSFPQL

The simulated poloidal density of the ICRF-heated species is such to *counteract* the centrifugal force acting on the high-Z impurities to avoid high-Z accumulation in the core.

(Odstrcil, PPCF 2018)

Outline

Separate Resonances in the Particle and Heat Fluxes: Quasilinear Model

Roughly (e.g. $v_\parallel k_\parallel$ is neglected)

High-Z Impurity Diffusivity

$$\frac{D^{\rm turb}_{Z,k}}{\rho_s^2\omega_{Dk}} \propto \int \frac{\hat\gamma_k}{\left(\hat\omega_k + \tau_Z \mathcal{K}_y \hat E_Z\right)^2 + \hat\gamma_k^2}\, e^{-\hat E_Z}\sqrt{\hat E_Z}\,{\rm d}\hat E_Z$$

Main-Ion Heat Conductivity

$$\frac{\chi^{\rm turb}_{ik}}{\rho_s^2\omega_{Dk}} \propto \int \frac{\hat\gamma_k}{\left(\hat\omega_k + \tau_i \mathcal{K}_y \hat E_Z\right)^2 + \hat\gamma_k^2}\, \hat E_i\left(\hat E_i - \frac{3}{2}\right) e^{-\hat E_i}\sqrt{\hat E_i}\,{\rm d}\hat E_i$$

with: $\tau_\sigma = T_\sigma/(Z_\sigma T_e)$; $\hat E_\sigma = E/T_\sigma$;
$\omega_{Dk} = k_y\rho_s(c_s/R)$ the fluid perpendicular drift frequency $(T = T_e)$;
$\mathcal{K}_y = -[\cos\theta + (s\theta - \alpha\sin\theta)\sin\theta]$ the bi-normal curvature (s–α);
$\hat\gamma_k = \gamma_k/\omega_{Dk}$ and $\hat\omega_k = \omega_k/\omega_{Dk}$: mode– growth rate and frequency.

(Angioni, PoP 2015)

Low–Frequency Modes Impact More the High-Z Impurity Transport Than the Heat Flux

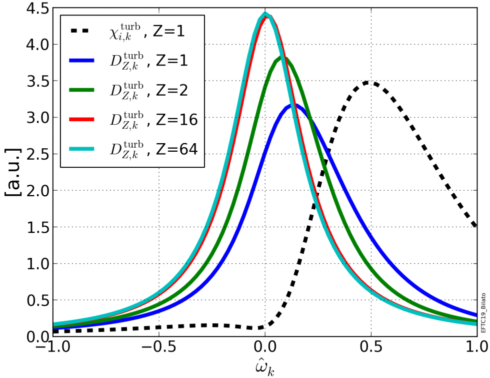

Low–Frequency Modes Impact More the High-Z Impurity Transport Than the Heat Flux

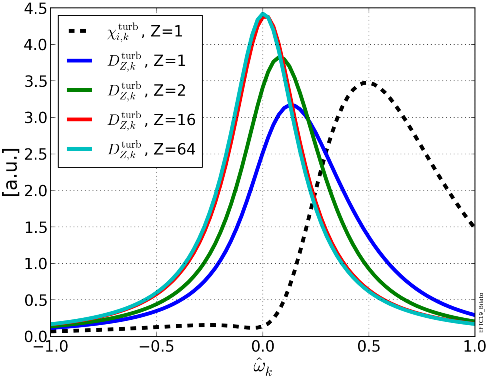

- The dependence on τ_Z of the drift frequency in the Lorentzian shifts the $D_{\rm Z,k}^{\rm turb}$ maximum to $\hat{\omega}_k \approx 0$ with increasing Z.

Low–Frequency Modes Impact More the High-Z Impurity Transport Than the Heat Flux

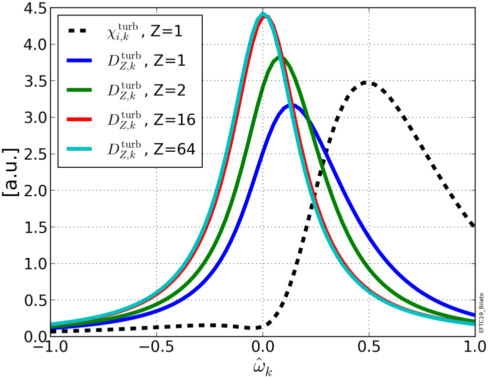

- The dependence on τ_Z of the drift frequency in the Lorentzian shifts the $D_{\mathrm{Z,k}}^{\mathrm{turb}}$ maximum to $\hat{\omega}_k \approx 0$ with increasing Z.
- The $\hat{\omega}_k$–shift between $D_{\mathrm{i,k}}^{\mathrm{turb}}$ and $\chi_{i,k}$ maxima is also consequence of the energy dependence of curvature and ∇B.

Low–Frequency Modes Impact More the High-Z Impurity Transport Than the Heat Flux

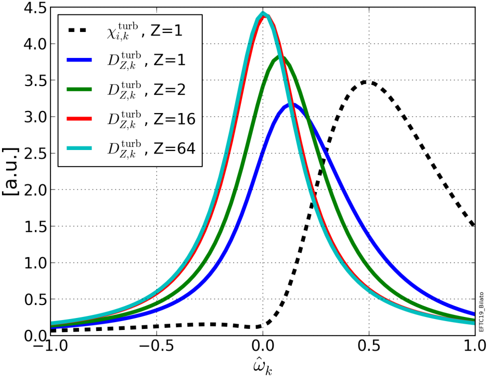

- The dependence on τ_Z of the drift frequency in the Lorentzian shifts the $D_{\rm Z,k}^{\rm turb}$ maximum to $\hat{\omega}_k \approx 0$ with increasing Z.
- The $\hat{\omega}_k$–shift between $D_{\rm i,k}^{\rm turb}$ and $\chi_{i,k}$ maxima is also consequence of the energy dependence of curvature and ∇B.

This $\hat{\omega}_r$–separation of the modes resonating in $D_{\rm Z}^{\rm turb}$ and in $\chi_{i,k}$ makes turbulence to counteract neoclassical inward convection without significantly impacting the main-ion heat flux, and thus the energy confinement performances.

(Angioni, NF 2017b)

Selectively Exciting Low-Frequency Modes: Experiments and Theory Insight – Design

Experimental observations

- Core RF (both EC and IC) heating helps in avoiding W core accumulation.

Experimental observations

- Core RF (both EC and IC) heating helps in avoiding W core accumulation.

⇓

Modeling for design&analysis

To address whether the physical mechanism behind EC and IC is the same, it is fundamental to have RF simulation tools to

- Design the discharges to have similar power deposition profiles of EC and IC;

Experimental observations

- Core RF (both EC and IC) heating helps in avoiding W core accumulation.

⇓

Modeling for design&analysis

To address whether the physical mechanism behind EC and IC is the same, it is fundamental to have RF simulation tools to

- Design the discharges to have similar power deposition profiles of EC and IC;
- Quantify Q_e/Q_i for further modeling.

Design of ASDEX-Upgrade experiments with comparable EC and IC heating profiles: TORBEAM code for EC and TORIC-SSFPQL for IC. $P_{\mathrm{NBI}} \approx 7.5$ MW.

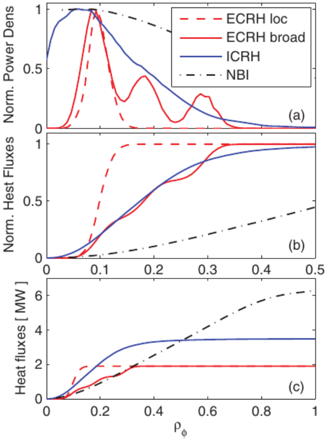

(Angioni, NF 2017a)

Selectively Exciting Low-Frequency Modes: Experiments and Theory Insight – Results

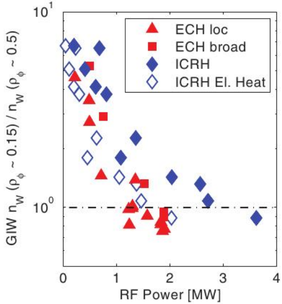

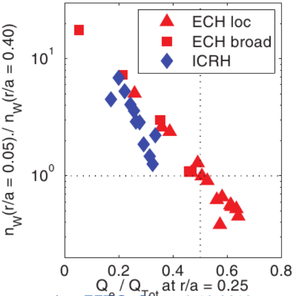

- To achieve the same W *reduction*, more ICRF is necessary than ECRF power.

Selectively Exciting Low-Frequency Modes: Experiments and Theory Insight – Results

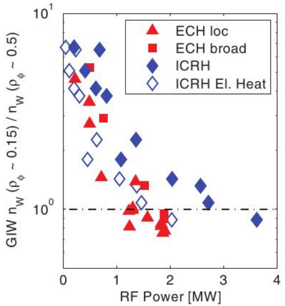

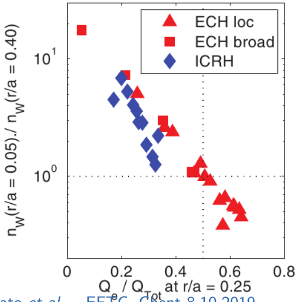

- To achieve the same W *reduction*, more ICRF is necessary than ECRF power.
- However, when the ICRF power absorbed by electrons (calculated with TORIC-SSFPQL) is considered, the W-accumulation dependence is similar to ECRF (blue-open diamonds vs red diamonds and squares).

Selectively Exciting Low-Frequency Modes: Experiments and Theory Insight – Results

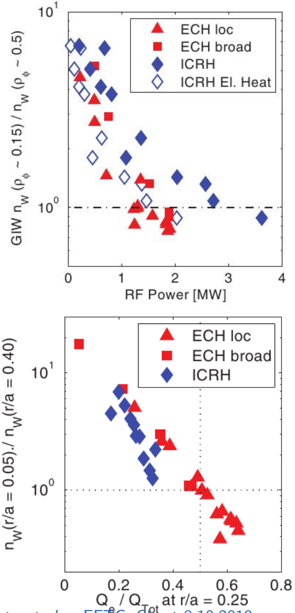

- To achieve the same W *reduction*, more ICRF is necessary than ECRF power.
- However, when the ICRF power absorbed by electrons (calculated with TORIC-SSFPQL) is considered, the W-accumulation dependence is similar to ECRF (blue-open diamonds vs red diamonds and squares).
- The *no-accumulation* state is achieved when $Q_e/Q_i \approx 1$.

Selectively Exciting Low-Frequency Modes: Experiments and Theory Insight – Results

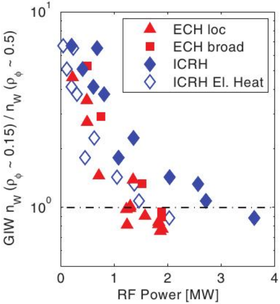

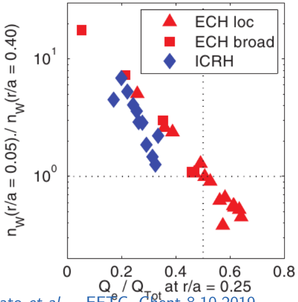

- To achieve the same W *reduction*, more ICRF is necessary than ECRF power.
- However, when the ICRF power absorbed by electrons (calculated with TORIC-SSFPQL) is considered, the W-accumulation dependence is similar to ECRF (blue-open diamonds vs red diamonds and squares).
- The *no-accumulation* state is achieved when $Q_e/Q_i \approx 1$.
- At the same Q_e/Q_i, ICRF heating is more effective, since it acts against the high-Z accumulation **also** by decreasing δ/ϵ and increasing η_i in the NC transp.

(Angioni, NF 2017a)

Selectively Exciting Low-Frequency Modes: Experiments and Theory Insight – Modeling

Gyrokinetic simulations with GKW code show that both W diffusion and W convection due to turbulence increase when $Q_e/Q_i \approx 1$.

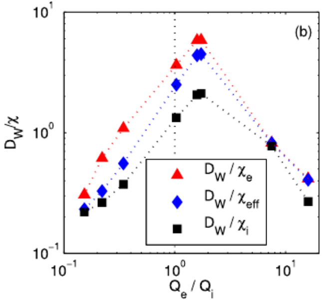

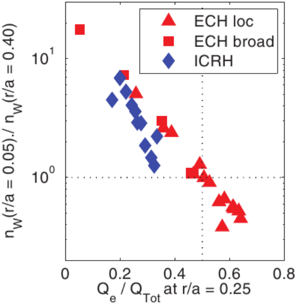

Eigenvalues solver of GKW code shows that in the region $Q_e/Q_i \approx 1$

- Turbulent W–diffusion is dominated by dominant ITG modes;
- Turbulent W–convection is dominated by sub-dominant TEM modes

(Angioni, PoP 2015, NF 2017a, NF 2017b)

Outline

Fast-Ion Effects on Plasma Turbulence

Stabilizing – Fast ions

Electrostatic:

- Dilute the thermal ITG drive;
- Resonate with ITG.

Electromagnetic :

- Geometrically stabilize via Shafranov shift;
- Mediate nonlinear energy transferred to high-frequency modes.

Destabilizing – Fast ions

Electromagnetic :

- drive instabilities through their pressure and its derivative.

(Di Siena, IAEA 2019)

Fast-Ion Effects on Plasma Turbulence

Stabilizing – Fast ions

Electrostatic:

- Dilute the thermal ITG drive;
- Resonate with ITG.

Electromagnetic :

- Geometrically stabilize via Shafranov shift;
- Mediate nonlinear energy transferred to high-frequency modes.

Destabilizing – Fast ions

Electromagnetic :

- drive instabilities through their pressure and its derivative.

(Di Siena, IAEA 2019)

Electrostatic Stabilization of ITG by Fast-Ions: Quasilinear Model

Approximating the distribution function with a Maxwellian (n_f, T_f)

Contribution of a minority species to the growth rate

$$\hat{\gamma}_f \propto n_f\,\tau_f \int \frac{\hat{\gamma}_k}{\left(\hat{\omega}_k + \tau_f \mathcal{K}_y \hat{E}_f\right)^2 + \hat{\gamma}_k^2} \left[1 + \eta_f \left(\hat{E}_f - \frac{3}{2}\right)\right] e^{-\hat{E}_f}\, \hat{E}_f^{3/2}\, \mathrm{d}\hat{E}_f$$

with: $\eta_f = L_n/L_{T_f}$; $\hat{E}_f = E/T_f$; $\tau_f = T_f/(Z_f T_e)$; $\hat{\omega}_k = \omega_k/\omega_{Dk}$; $\hat{\gamma}_{k,f} = \gamma_{k,f}/\omega_{Dk}$;
$\omega_{Dk} = k_y \rho_s (c_s/R)$; $\mathcal{K}_y = -[\cos\theta + (s\theta - \alpha\sin\theta)\sin\theta]$.

Electrostatic Stabilization of ITG by Fast-Ions: Quasilinear Model

Approximating the distribution function with a Maxwellian (n_f, T_f)

Contribution of a minority species to the growth rate

$$\hat{\gamma}_f \propto n_f \, \tau_f \int \frac{\hat{\gamma}_k}{\left(\hat{\omega}_k + \tau_f \mathcal{K}_y \hat{E}_f\right)^2 + \hat{\gamma}_k^2} \left[1 + \eta_f \left(\hat{E}_f - \frac{3}{2}\right)\right] e^{-\hat{E}_f} \, \hat{E}_f^{3/2} \, \mathrm{d}\hat{E}_f$$

with: $\eta_f = L_n / L_{T_f}$; $\hat{E}_f = E/T_f$; $\tau_f = T_f/(Z_f T_e)$; $\hat{\omega}_k = \omega_k/\omega_{Dk}$; $\hat{\gamma}_{k,f} = \gamma_{k,f}/\omega_{Dk}$;
$\omega_{Dk} = k_y \rho_s (c_s/R)$; $\mathcal{K}_y = -[\cos\theta + (s\theta - \alpha\sin\theta)\sin\theta]$.

- "Fast ions" $\Longrightarrow \tau_f \gg 1$ (**Note:** before $\tau_Z \ll 1$ due to $Z \gg 1$!).

Electrostatic Stabilization of ITG by Fast-Ions: Quasilinear Model

Approximating the distribution function with a Maxwellian (n_f, T_f)

Contribution of a minority species to the growth rate

$$\hat{\gamma}_f \propto n_f\,\tau_f \int \frac{\hat{\gamma}_k}{\left(\hat{\omega}_k + \tau_f \mathcal{K}_y \hat{E}_f\right)^2 + \hat{\gamma}_k^2} \left[1 + \eta_f \left(\hat{E}_f - \frac{3}{2}\right)\right] e^{-\hat{E}_f}\, \hat{E}_f^{3/2}\, \mathrm{d}\hat{E}_f$$

with: $\eta_f = L_n/L_{T_f}$; $\hat{E}_f = E/T_f$; $\tau_f = T_f/(Z_f T_e)$; $\hat{\omega}_k = \omega_k/\omega_{Dk}$; $\hat{\gamma}_{k,f} = \gamma_{k,f}/\omega_{Dk}$;
$\omega_{Dk} = k_y \rho_s (c_s/R)$; $\mathcal{K}_y = -[\cos\theta + (s\theta - \alpha\sin\theta)\sin\theta]$.

- "Fast ions" $\Longrightarrow \tau_f \gg 1$ (**Note:** before $\tau_Z \ll 1$ due to $Z \gg 1$!).
- Resonance condition: $\hat{E}_f \approx \hat{E}_{f,\mathrm{res}} = \hat{\omega}_k / \big((-\mathcal{K}_y)\tau_f\big)$.

Approximating the distribution function with a Maxwellian (n_f, T_f)

Contribution of a minority species to the growth rate

$$\hat{\gamma}_f \propto n_f \, \tau_f \int \frac{\hat{\gamma}_k}{\left(\hat{\omega}_k + \tau_f \mathcal{K}_y \hat{E}_f\right)^2 + \hat{\gamma}_k^2} \left[1 + \eta_f \left(\hat{E}_f - \frac{3}{2}\right)\right] e^{-\hat{E}_f} \, \hat{E}_f^{3/2} \, \mathrm{d}\hat{E}_f$$

with: $\eta_f = L_n / L_{T_f}$; $\hat{E}_f = E/T_f$; $\tau_f = T_f/(Z_f T_e)$; $\hat{\omega}_k = \omega_k/\omega_{Dk}$; $\hat{\gamma}_{k,f} = \gamma_{k,f}/\omega_{Dk}$;
$\omega_{Dk} = k_y \rho_s (c_s/R)$; $\mathcal{K}_y = -[\cos\theta + (s\theta - \alpha \sin\theta)\sin\theta]$.

- "Fast ions" $\Longrightarrow \tau_f \gg 1$ (**Note:** before $\tau_Z \ll 1$ due to $Z \gg 1$!).
- Resonance condition: $\hat{E}_f \approx \hat{E}_{f,\mathrm{res}} = \hat{\omega}_k / \big((-\mathcal{K}_y)\tau_f\big)$.
- When $\eta_f > 0$, resonating ions stabilize $(\hat{\gamma}_v < 0)$ if

$$0 \lesssim \hat{E}_{\mathrm{f,res}} \lesssim \hat{E}_{\mathrm{f,crt}}, \qquad \text{with :} \quad \hat{E}_{f,\mathrm{crt}} = \frac{3}{2} - \frac{1}{\eta_f}$$

Approximating the distribution function with a Maxwellian (n_f, T_f)

Contribution of a minority species to the growth rate

$$\hat{\gamma}_f \propto n_f\,\tau_f \int \frac{\hat{\gamma}_k}{\left(\hat{\omega}_k + \tau_f \mathcal{K}_y \hat{E}_f\right)^2 + \hat{\gamma}_k^2} \left[1 + \eta_f \left(\hat{E}_f - \frac{3}{2}\right)\right] e^{-\hat{E}_f}\, \hat{E}_f^{3/2}\, \mathrm{d}\hat{E}_f$$

with: $\eta_f = L_n/L_{T_f}$; $\hat{E}_f = E/T_f$; $\tau_f = T_f/(Z_f T_e)$; $\hat{\omega}_k = \omega_k/\omega_{Dk}$; $\hat{\gamma}_{k,f} = \gamma_{k,f}/\omega_{Dk}$;
$\omega_{Dk} = k_y \rho_s (c_s/R)$; $\mathcal{K}_y = -[\cos\theta + (s\theta - \alpha\sin\theta)\sin\theta]$.

- "Fast ions" $\Longrightarrow \tau_f \gg 1$ (**Note:** before $\tau_Z \ll 1$ due to $Z \gg 1$!).
- Resonance condition: $\hat{E}_f \approx \hat{E}_{f,\mathrm{res}} = \hat{\omega}_k / \big((-\mathcal{K}_y)\tau_f\big)$.
- When $\eta_f > 0$, resonating ions stabilize $(\hat{\gamma}_v < 0)$ if

$$0 \lesssim \hat{E}_{\mathrm{f,res}} \lesssim \hat{E}_{\mathrm{f,crt}}, \qquad \text{with :} \quad \hat{E}_{f,\mathrm{crt}} = \frac{3}{2} - \frac{1}{\eta_f}$$

- Typically $\eta_{\mathrm{NBI}} \ll 1$ and $\hat{E}_{\mathrm{f,crt}} \ll 1 \Longrightarrow$ negligible stabilization

(Di Siena, NF 2018, PoP 2019)

Electrostatic Stabilization of ITG by Fast-Ions: Predictions of the Quasilinear Model

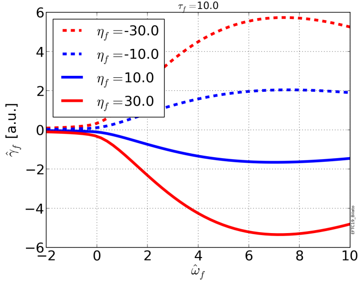

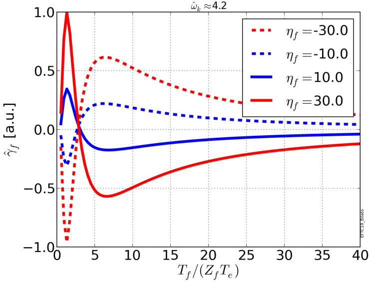

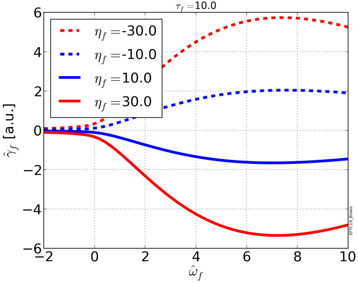

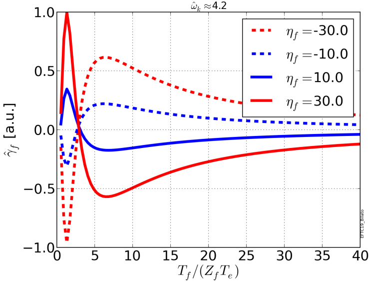

When $\eta_f \gg 1$:

- Stabilization of ITGs, stronger for $\hat{\omega}_k \gg 1$.

Electrostatic Stabilization of ITG by Fast-Ions: Predictions of the Quasilinear Model

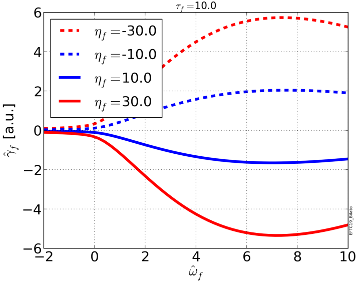

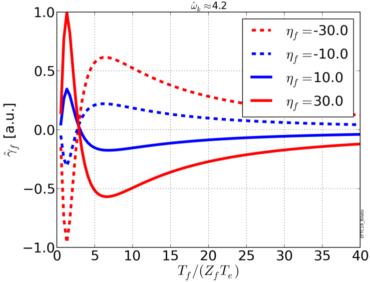

When $\eta_f \gg 1$:

- Stabilization of ITGs, stronger for $\hat{\omega}_k \gg 1$.
- Reduced impact on TEMs ($\omega_r < 0$), especially when $\gamma_k/\omega_{\mathrm{Di}} \ll 1$.

Electrostatic Stabilization of ITG by Fast-Ions: Predictions of the Quasilinear Model

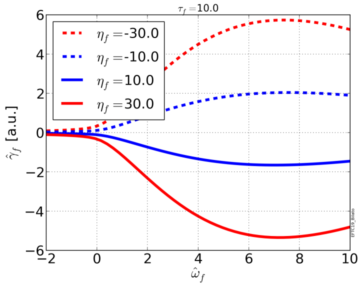

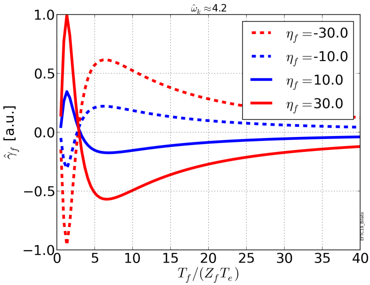

When $\eta_f \gg 1$:

- Stabilization of ITGs, stronger for $\hat{\omega}_k \gg 1$.
- Reduced impact on TEMs ($\omega_r < 0$), especially when $\gamma_k/\omega_{\rm Di} \ll 1$.
- Existence of an optimal range of $\tau_f = T_f/(Z_f T_e)$.

Electrostatic Stabilization of ITG by Fast-Ions: Predictions of the Quasilinear Model

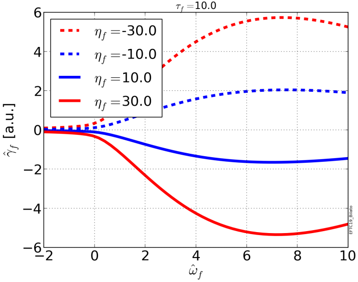

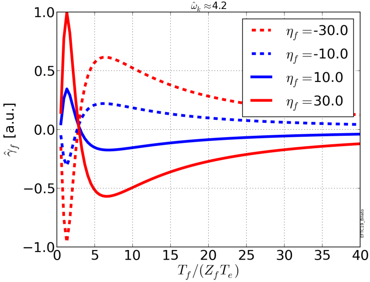

When $\eta_f \gg 1$:

- Stabilization of ITGs, stronger for $\hat{\omega}_k \gg 1$.
- Reduced impact on TEMs ($\omega_r < 0$), especially when $\gamma_k/\omega_{\mathrm{Di}} \ll 1$.
- Existence of an optimal range of $\tau_f = T_f/(Z_f T_e)$.

ICRF ($\eta_f \gg 1$) via this mechanism might reduce the turbulent main-ion heat and particle fluxes, without substantially reducing the subdominant TEMs and low–ω_r ITGs, important for flushing the high-Z ions.

Impact of a Minority-Fast-Ion Species on the micro-instabilities: GENE

ITG growth rates

GENE linear simulations

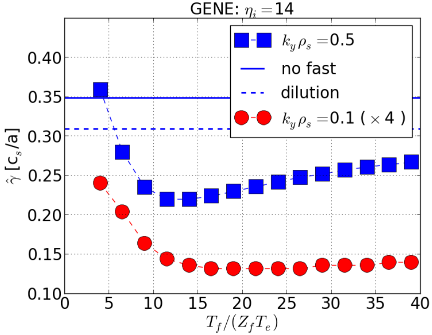

Rescaled quasilinear expression

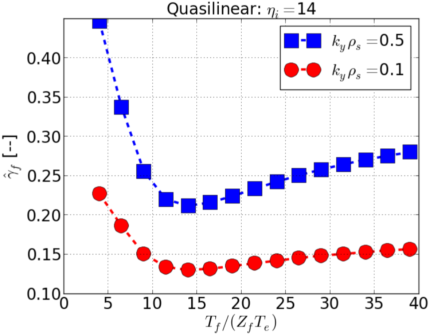

ITG growth rates

GENE linear simulations

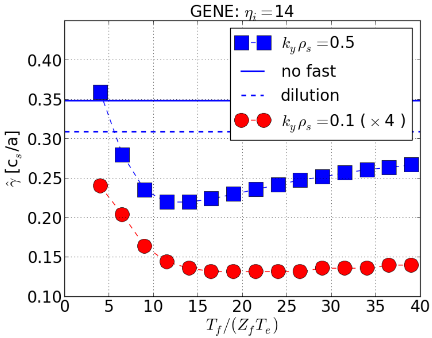

Rescaled quasilinear expression

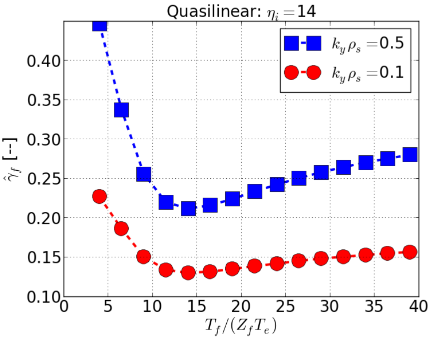

Qualitativaly:

the QL model captures the dependence on η_f, τ_f and $k_y \rho_i$, shading light on the role of this resonant mechanism in the linear GENE simulations.

(Di Siena, NF 2018, PoP 2019)

Outline

1. Ion-Cyclotron Radio-Frequency (ICRF) heating
   - Modeling wave propagation & absorption
2. Impact of ICRF heating on the radial high-Z impurity transport
   - Neoclassical: T_i gradient and poloidal density asymmetries
   - Turbulence: affecting the electron to ion heat flux ratio
3. Effects of ICRF-accelerated fast ions on turbulence
   - ITG stabilization and T_i steepening in AUG discharge
   - Application to ITER
4. Validation (outlook)
5. Summary

ICRF Stabilization in AUG Discharges: ASTRA

- ICRF ^{3}He–minority in D plasmas: this mechanism can explain 40% of the excess of GENE predictions of Q_i w.r.t. experimental estimates.
  (Bonanomi, NF 2018)
- ICRF H–minority in D plasmas: recent experiments on AUG shows a steepening of T_i in correspondence of the region of maximum η_f and T_f, calculated by TORIC-SSFPQL:

Experimental T_i

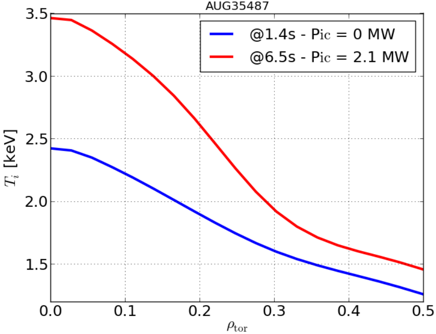

ASTRA (+TGLF) + TORIC-SSFPQL

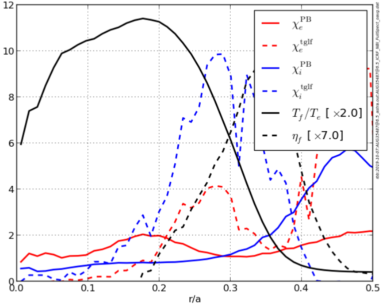

(Fable, PPCF 2013; Staebler NF 2017)

ICRF Stabilization in AUG Discharges: GENE

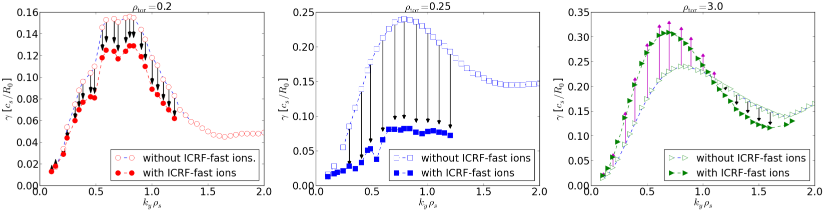

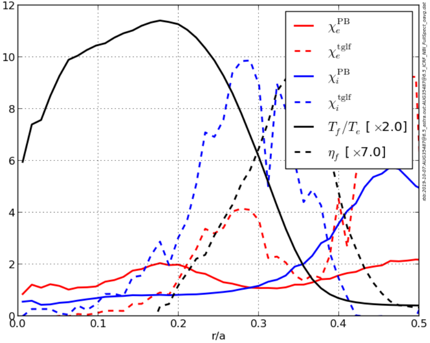

ICRF Stabilization in AUG Discharges: GENE

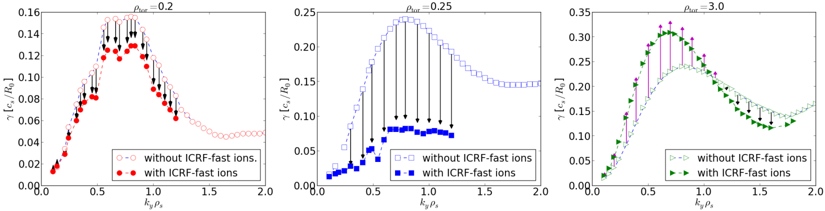

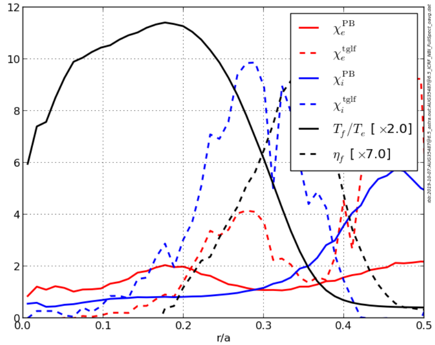

- For $\rho_{\rm tor} \lesssim 0.25$, ASTRA(TGLF) *without* fast ions predicts χ_i much larger than the power balance values ($\chi_i^{\rm PB}$).

ICRF Stabilization in AUG Discharges: GENE

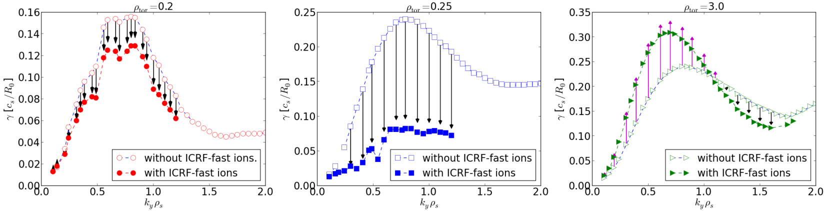

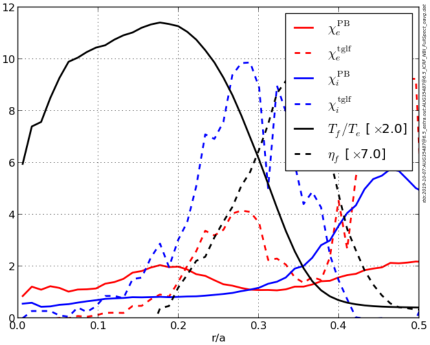

- For $\rho_{tor} \lesssim 0.25$, ASTRA(TGLF) *without* fast ions predicts χ_i much larger than the power balance values (χ_i^{PB}).
- Linear GENE results show that around the largest η_f ITGs are strongly stabilized ($\rho_{tor} \approx 0.25$).

ICRF Stabilization in AUG Discharges: GENE

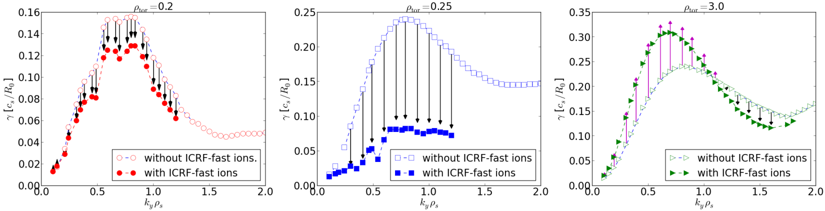

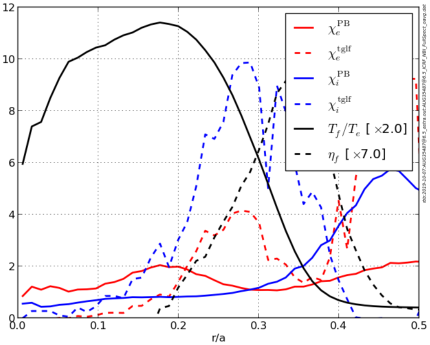

- For $\rho_{tor} \lesssim 0.25$, ASTRA(TGLF) *without* fast ions predicts χ_i much larger than the power balance values (χ_i^{PB}).
- Linear GENE results show that around the largest η_f ITGs are strongly stabilized ($\rho_{tor} \approx 0.25$).
- *Preliminary* nonlinear global GENE results $\Longrightarrow$ reduction of the main ion heat flux, Q_i.

Outline

ICRF Scheme in ITER at Full-Field

- $B_0 = 5.2$ Tesla, $f_{\rm ic} = 51$ MHz, D-T(^{3}He) ICRF scheme: in the intial phase ($T \lesssim 10$ keV) $\Longrightarrow$ energetic ICRF-^{3}He tails.

Linear growth rate

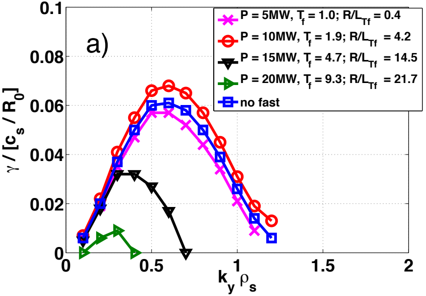

Nonlinear main ion heat flux

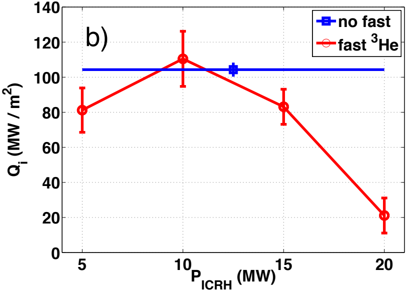

- $B_0 = 5.2$ Tesla, $f_{\rm ic} = 51$ MHz, D-T(^{3}He) ICRF scheme: in the intial phase ($T \lesssim 10$ keV) $\Longrightarrow$ energetic ICRF-^{3}He tails.

Linear growth rate | Nonlinear main ion heat flux

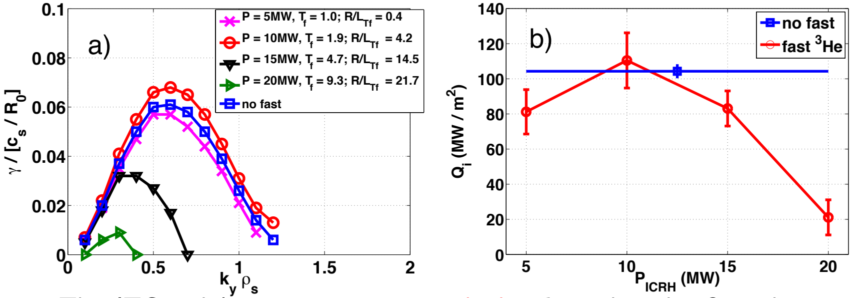

- This ITG stabilization is stronger at higher $k_y\rho_s$, but the Q_i–reduction is more sensitive to low $k_y\rho_s$ modes

ICRF Scheme in ITER at Full-Field

- $B_0 = 5.2$ Tesla, $f_{\rm ic} = 51$ MHz, D-T(^{3}He) ICRF scheme: in the intial phase ($T \lesssim 10$ keV) $\Longrightarrow$ energetic ICRF-^{3}He tails.

Linear growth rate

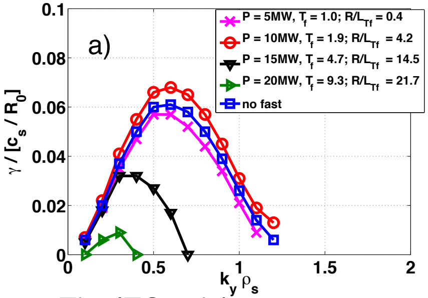

Nonlinear main ion heat flux

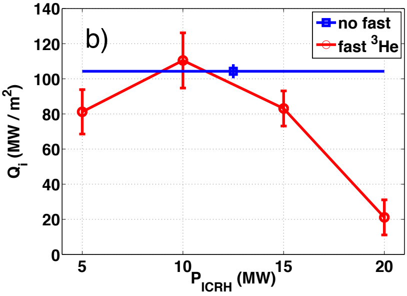

- This ITG stabilization is stronger at higher $k_y\rho_s$, but the Q_i–reduction is more sensitive to low $k_y\rho_s$ modes

This stabilization mechanism might help in the initial phase of the discharge.

(Di Siena, NF 2018)

Outline

Validation of the Computed Distribution Function on AUG

- TORIC: intensively benchmarked and validated, thanks also to the worldwide used TRANSP suite.

Validation of the Computed Distribution Function on AUG

- TORIC: intensively benchmarked and validated, thanks also to the worldwide used TRANSP suite.
- SSFPQL: more challenging – good NBI-only, recent improvements ICRF-only, in progress ICRF+NBI.

Validation of the Computed Distribution Function on AUG

- TORIC: intensively benchmarked and validated, thanks also to the worldwide used TRANSP suite.
- SSFPQL: more challenging – good NBI-only, recent improvements ICRF-only, in progress ICRF+NBI.

CXRS diagnostics

3-ion scheme, H-D(^{3}He)

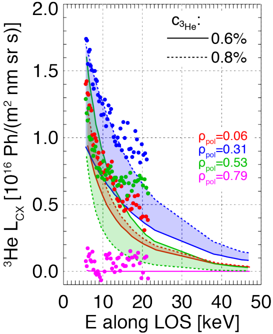

(A. Kappatou, this conference, I.04)

Fast Ion D-alpha diagnostics

D(H) minority ICRF scheme

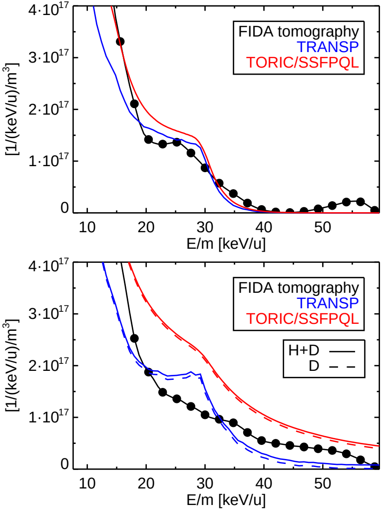

(Pankin, CPC 2004) (Weiland, NF 2017)

Outline

1. Ion-Cyclotron Radio-Frequency (ICRF) heating
   - Modeling wave propagation & absorption
2. Impact of ICRF heating on the radial high-Z impurity transport
   - Neoclassical: T_i gradient and poloidal density asymmetries
   - Turbulence: affecting the electron to ion heat flux ratio
3. Effects of ICRF-accelerated fast ions on turbulence
   - ITG stabilization and T_i steepening in AUG discharge
   - Application to ITER
4. Validation (outlook)
5. **Summary**

Summary

Interconnecting simulation tools for

1. ICRF (here: `TORIC-SSFPQL`)
2. Transport (here: `ASTRA(+TGLF)`)
3. Gyrokinetics (here: `GENE` and `GKW`)

helps to design & analyze the present and future experiments using ICRF to

Summary

Interconnecting simulation tools for

1. ICRF (here: `TORIC-SSFPQL`)
2. Transport (here: `ASTRA(+TGLF)`)
3. Gyrokinetics (here: `GENE` and `GKW`)

helps to design & analyze the present and future experiments using ICRF to

- impact the high-Z impurity radial transport by

Summary

Interconnecting simulation tools for

1. ICRF (here: `TORIC-SSFPQL`)
2. Transport (here: `ASTRA(+TGLF)`)
3. Gyrokinetics (here: `GENE` and `GKW`)

helps to design & analyze the present and future experiments using ICRF to

- impact the high-Z impurity radial transport by
  - **reducing** the inward *neoclassical* convection through the
    - increase of the temperature screening contribution ($\eta_i \uparrow$);
    - decrease of the out-in asymmetry ($\delta/\epsilon \downarrow$) due to centrifugal forces
      $\Longrightarrow$This effect is limited to slow-rotating plasmas (e.g. ITER).

Summary

Interconnecting simulation tools for

1. ICRF (here: `TORIC-SSFPQL`)
2. Transport (here: `ASTRA(+TGLF)`)
3. Gyrokinetics (here: `GENE` and `GKW`)

helps to design & analyze the present and future experiments using ICRF to

- impact the high-Z impurity radial transport by
  - **reducing** the inward *neoclassical* convection through the
    - increase of the temperature screening contribution ($\eta_i \uparrow$);
    - decrease of the out-in asymmetry ($\delta/\epsilon \downarrow$) due to centrifugal forces
      $\Longrightarrow$This effect is limited to slow-rotating plasmas (e.g. ITER).
  - **increasing** turbulent diffusion and convection of high-Z impurities without substantially increase the heat fluxes of the main ions.

Summary

Interconnecting simulation tools for

1. ICRF (here: `TORIC-SSFPQL`)
2. Transport (here: `ASTRA(+TGLF)`)
3. Gyrokinetics (here: `GENE` and `GKW`)

helps to design & analyze the present and future experiments using ICRF to

- impact the high-Z impurity radial transport by
  - **reducing** the inward *neoclassical* convection through the
    - increase of the temperature screening contribution ($\eta_i \uparrow$);
    - decrease of the out-in asymmetry ($\delta/\epsilon \downarrow$) due to centrifugal forces
      $\Longrightarrow$This effect is limited to slow-rotating plasmas (e.g. ITER).
  - **increasing** turbulent diffusion and convection of high-Z impurities without substantially increase the heat fluxes of the main ions.
- stabilize ITG turbulence by

Summary

Interconnecting simulation tools for

1. ICRF (here: `TORIC-SSFPQL`)
2. Transport (here: `ASTRA(+TGLF)`)
3. Gyrokinetics (here: `GENE` and `GKW`)

helps to design & analyze the present and future experiments using ICRF to

- impact the high-Z impurity radial transport by
  - **reducing** the inward *neoclassical* convection through the
    - increase of the temperature screening contribution ($\eta_i \uparrow$);
    - decrease of the out-in asymmetry ($\delta/\epsilon \downarrow$) due to centrifugal forces
      $\Longrightarrow$This effect is limited to slow-rotating plasmas (e.g. ITER).
  - **increasing** turbulent diffusion and convection of high-Z impurities without substantially increase the heat fluxes of the main ions.
- stabilize ITG turbulence by
  - **creating** fast ions resonating mainly with ITG modes.
    $\Longrightarrow$ In ITER this mechanism might play a beneficial role in the initial phase of the discharge.

Cited references

Angioni, PPCF 2014: C. Angioni *et al*, PPCF, **56** (2014) 124001.

Angioni, PoP 2015: C. Angioni, PoP, **22** (2015) 102501.

Angioni, NF 2017a: C. Angioni *et al*, NF, **57** (2017) 022009.

Angioni, NF 2017b: C. Angioni *et al*, NF, **57** (2017) 056015.

Belmondo, JoP 2010: V. Belmondo *et al*, JoP, **260** 012001.

Bilato, NF 2002: R. Bilato *et al*, NF, **42** (2002) 1085.

Bilato, NF 2011: R. Bilato *et al*, NF, **51** (2011) 103034.

Bilato, JoP 2012: R. Bilato *et al*, JoP, **401** (2012) 012001.

Bilato, NF 2014: R. Bilato *et al*, NF, **54** (2014) 072003.

Bilato, JoP 2014: R. Bilato *et al*, JoP, **561** (2014) 012001.

Bilato, NF 2017a: R. Bilato *et al*, NF, **57** (2017) 056020.

Bilato, NF 2017b: R. Bilato *et al*, NF, **57** (2017) 076017.

Bonanomi, NF 2018: N. Bonanomi *et al*, NF, **58** (2018) 056025.

Brambilla, NF 1994: M. Brambilla *et al*, NF, **34** (1994) 1121.

Brambilla, PPCF 1999: M. Brambilla *et al*, PPCF, **41** (1999) 1.

Brambilla, NF 2009: M. Brambilla *et al*, NF, **49** (2009) 085004.

Brambilla, CPC 2009: M. Brambilla *et al*, CPC, **184** (2013) 2053.

Brambilla, NF 2015: M. Brambilla *et al*, NF, **55** (2015) 023016.

Casson, PPCF 2015: F. J. Casson *et al*, PPCF, **57** (2015) 014031.

Cited references (con't)

Ehst, NF 1991: D. A. Ehst *et al*, NF, **31** (1991) 1933.

Di Siena, NF 2018: A. Di Siena *et al*, NF, **58** (2018) 054002.

Di Siena, PoP 2019: A. Di Siena *et al*, PoP, **26** (2019) 052504.

Di Siena, IAEA 2019: A. Di Siena *et al*, `https://conferences.iaea.org/indico/event/185/contributions/14944/attachments/8105/10681/I-3_DiSiena_IAEA_2019.pdf`

Fable, PPCF 2013: E. Fable *et al*, PPCF, **55** (2013) 124028.

Feng, CPC 1995: Y. Feng *et al*, CPC, **88** (2995) 161.

Helander&Sigmar : P. Helander & D.J. Sigmar, "Collisional Transport in Magnetized Plasmas", Cambridge Univ. Press, (2002).

Kazakov, Nature Phsyics 2017: Ye. O. Kazakov *et al*, Nature Phsyics, **13** (2017) 973.

Kiptily, NF 2005: V.G. Kiptily *et al*, NF, **45** (2005) L21-L25.

Odstrcil, PPCF 2018: T. Odstrcil *et al*, PPCF, **60** (2018) 014003.

Pankin, CPC 2004: A. Pankin *et al*, CPC, **159** (2004) 157.

Polevoi, IAEA 2019: A. Polevoi *et al*, `https://conferences.iaea.org/indico/event/185/contributions/14942/attachments/8096/10672/ID7-POLEVOI.pdf`

Reinke, PPCF 2012: M. L. Reinke *et al*, PPCF, **54** (2012) 045004.

Staeble, NF 2017: G. M. Staebler *et al*, NF, **57** (2017) 066046.

Weiland, NF 2017; M. Weiland *et al*, NF, **57** (2017) 116058.

NF = Nuclear Fusion; PPCF = Plasma Physics and Controlled Fusion; PoP = Physics of Plasmas; JoP = Journal of Physics: Conference Series; CPC = Computer Physics Communications.